PERTURBATIVE QCD

W.J. Stirling

Departments of Mathematical Sciences and Physics,
University of Durham,
South Road, Durham DH1 3LE, UK

Abstract

Some of the basic concepts and most important results of perturbative QCD are presented, together with some illustrative comparisons with experiment.

1. INTRODUCTION

Quantum Chromodynamics (QCD), the gauge field theory that describes the interactions of coloured quarks and gluons, is one of the components of the SU(3)×SU(2)×U(1) Standard Model. At short distances, equivalently high energies, the effective coupling is small and the theory can be studied using perturbative techniques. Nowadays detailed tests of perturbative QCD are performed at all the high-energy colliders, and in the production and decay of heavy quark systems. Some of the most direct information comes from high-energy processes involving leptons and photons. The colour neutrality of these particles, together with the relative ease with which they can be accelerated and detected in experiments, allows for particularly precise theoretical calculations and experimental measurements. The paradigm process is the investigation of the short-distance structure of hadrons using virtual electroweak gauge boson probes ($\gamma, W^\pm, Z^0$) emitted from high-energy beams of charged leptons or neutrinos — deep inelastic scattering. Here we see the asymptotic property directly, as the gauge bosons scatter incoherently off the weakly interacting quarks and gluons, for example $\gamma^* q \to q$ and $\gamma^* g \to q\bar{q}$. From such experiments we learn how the partons (i.e. the quarks and gluons) share the momentum and quantum numbers of the hadron. By studying how the 'structure functions' vary with the momentum transferred by the probe, precision measurements of the short-distance coupling can be made. The information obtained in this way is a vital input to signal and background cross–section calculations at the LHC.

Another fundamental QCD process is the production of hadrons in electron–positron annihilation, $e^+e^- \to q\bar{q}$ at lowest order. The importance of this process is that it allows a detailed study of how quarks 'shower' into multiparton states, and how these materialize into jets of hadrons. The quark and gluon spins, the non–Abelian vertices of the theory and the short-distance coupling can be measured from these final states.

In these lectures we will discuss these and other high-energy processes, with the common theme of providing detailed phenomenological tests of perturbative QCD. Much of the basic theoretical framework is covered in the lectures by Bardin, but to make the discussion relatively self–contained, we first of all (Section 2) review some of the fundamental properties of the theory that are particularly relevant for the processes under consideration. Of particular importance in this context is the definition of the 'running' coupling α_S, the fundamental parameter of the theory, and the colour algebra identities that are necessary for performing calculations. In Section 3 we review the application of perturbative QCD to high-energy electron-positron annihilation, focusing in particular on the total cross section and multijet final states. In Section 4 we introduce the parton model of short–distance hadron structure and discuss how the basic 'scaling' property is modified by perturbative QCD corrections, and how parton distributions can be determined from experiment. Some applications to high–energy hadron collider processes are discussed in Section 5.

Lack of space precludes an in–depth treatment of most of these issues, but further information can of course be found in the literature. In particular, Ref. [1] covers all the topics discussed in these lectures in significantly greater detail.

2. BASICS OF PERTURBATIVE QCD

2.1 The QCD Lagrangian

The QCD Lagrangian is, up to gauge–fixing terms,

$$\begin{aligned}
\mathcal{L}_{QCD} &= -\frac{1}{4}F_{\mu\nu}^{(a)}F^{(a)\mu\nu} + \sum_q \bar{\psi}_i^q \left(i\gamma^\mu(D_\mu)_{ij} - m_q\delta_{ij}\right)\psi_j^q \\
F_{\mu\nu}^{(a)} &= \partial_\mu A_\nu^a - \partial_\nu A_\mu^a + g_s f_{abc}A_\mu^b A_\nu^c \\
(D_\mu)_{ij} &= \delta_{ij}\partial_\mu - ig_s T_{ij}^a A_\mu^a
\end{aligned} \tag{1}$$

where g_s is the QCD coupling constant, T_{ij}^a and f_{abc} are the SU(3) colour matrices and structure constants respectively, the $\psi_i^q(x)$ are the 4–component Dirac spinors associated with each quark field of colour i and flavour q, and the $A_\mu^a(x)$ are the eight Yang-Mills gluon fields. From this Lagrangian, the Feynman rules can be derived in the usual way, see the Table on the next page, which is reproduced from Ref. [1].

Explicit forms for the SU(3) colour matrices and structure constants can be found, for example, in Ref. [1]. The following are some useful identities:

$$\begin{aligned}
[T^a, T^b] &= if^{abc}T^c \\
\{T^a, T^b\} &= d^{abc}T^c + \frac{1}{3}\delta^{ab} \\
f^{acd}f^{bcd} &= C_A\delta^{ab} \\
(T^aT^a)_{ij} = T_{ik}^a T_{kj}^a &= C_F\delta_{ij} \\
\mathrm{Tr}(T^aT^b) = T_{ij}^a T_{ji}^b &= T_F\delta^{ab} \\
C_A &= N_c = 3 \\
C_F &= \frac{N_c^2 - 1}{2N_c} = \frac{4}{3} \\
T_F &= \frac{1}{2} \\
\mathrm{Tr}(T^aT^bT^c) &= \frac{i}{4}f^{abc} + \frac{1}{4}d^{abc} \\
f^{abc}f^{abc} &= 24 \\
d^{abc}d^{abc} &= \frac{40}{3}
\end{aligned} \tag{2}$$

where summation over repeated indices is understood.

2.2 The QCD coupling constant

Quantum Chromodynamics is an asymptotically free gauge field theory, that is, the strength of the interaction between the quarks and gluons becomes weaker in the short–distance limit. In QCD the renormalized coupling can be defined in a variety of ways, for example from the 'dressed' qqg or ggg vertices. Renormalization of the coupling necessitates the introduction of a scale μ — effectively the scale at which the ultra–violet loop divergences are subtracted off. A dimensionless physical quantity R that depends on some energy scale Q will depend also on μ both *explicitly* and *implicitly* through the renormalized coupling, i.e. $R = R(\mu^2/Q^2, \alpha_S(\mu^2))$. The fact that such a quantity should not depend on the arbitrary scale μ (when calculated to all orders in perturbation theory) leads to an equation for the μ dependence of the renormalized coupling:

$$\frac{\mu^2}{\alpha_S(\mu^2)}\frac{\partial \alpha_S(\mu^2)}{\partial \mu^2} = -\frac{\alpha_S(\mu^2)}{4\pi}\beta_0 - \left(\frac{\alpha_S(\mu^2)}{4\pi}\right)^2\beta_1 - \left(\frac{\alpha_S(\mu^2)}{4\pi}\right)^3\beta_2 + ...$$

Table 1: Feynman rules for QCD in a covariant gauge.

A, α p B, β

$$\delta^{AB} \left[-g^{\alpha\beta} + (1-\lambda)\frac{p^\alpha p^\beta}{p^2 + i\varepsilon} \right] \frac{i}{p^2 + i\varepsilon}$$

A p B

$$\delta^{AB} \frac{i}{p^2 + i\varepsilon}$$

a, i p b, j

$$\delta^{ab} \frac{i}{(\hat{p} - m + i\varepsilon)_{ji}}$$

B, β

q

p r

A, α C, γ

$$-gf^{ABC} \left[g^{\alpha\beta}(p-q)^\gamma + g^{\beta\gamma}(q-r)^\alpha \right.$$
$$\left. + g^{\gamma\alpha}(r-p)^\beta \right]$$
(all momenta incoming)

A, α B, β

C, γ D, δ

$$-ig^2 f^{XAC} f^{XBD} (g_{\alpha\beta}g_{\gamma\delta} - g_{\alpha\delta}g_{\beta\gamma})$$
$$-ig^2 f^{XAD} f^{XBC} (g_{\alpha\beta}g_{\gamma\delta} - g_{\alpha\gamma}g_{\beta\delta})$$
$$-ig^2 f^{XAB} f^{XCD} (g_{\alpha\gamma}g_{\beta\delta} - g_{\alpha\delta}g_{\beta\gamma})$$

A, α

q

B C

$$gf^{ABC}q^\alpha$$

A, α

b, i c, j

$$-ig \left(T^A \right)_{cb} (\gamma^\alpha)_{ji}$$

$$\beta_0 = 11 - \frac{2}{3}n_f$$

$$\beta_1 = 102 - \frac{38}{3}n_f$$

$$\beta_2(\overline{\text{MS}}) = \frac{2857}{2} - \frac{5033}{18}n_f + \frac{325}{54}n_f^2, \tag{3}$$

for n_f massless quark flavours. Note that the coefficients in the above perturbative expansion depend, in general, on the renormalization scheme (RS), although for massless quarks the first two coefficients, β_0 and β_1, are RS independent. In essentially all phenomenological applications the $\overline{\text{MS}}$ RS is used.

At leading order, i.e. retaining only the coefficient β_0, Eq. (3) can be solved for α_S to give

$$\alpha_S(\mu^2) = \frac{\alpha_S(\mu_0^2)}{1 + \alpha_S(\mu_0^2)\, b \ln(\mu^2/\mu_0^2)} \tag{4}$$

or

$$\alpha_S(\mu^2) = \frac{1}{b \ln(\mu^2/\Lambda^2)}, \tag{5}$$

where $b = \beta_0/4\pi = (33 - 2n_f)/(12\pi)$.

These two expressions are entirely equivalent — they differ only in the choice of boundary condition for the differential equation, $\alpha_S(\mu_0^2)$ in the first case and the dimensionful parameter Λ in the second. In fact nowadays Λ is disfavoured as the fundamental parameter of QCD, since its definition is not unique beyond leading order (see below), and its value depends on the number of 'active' quark flavours. Instead, it has become conventional to use the value of α_S in the $\overline{\text{MS}}$ scheme at $\mu^2 = M_Z^2$ as the fundamental parameter. The advantage of using M_Z as the reference scale is that it is (a) very precisely measured [2], (b) safely in the perturbative regime, i.e. $\alpha_S(M_Z^2) \ll 1$, and (c) far from quark thresholds, i.e. $m_b \ll M_Z \ll m_t$.

The parameter Λ is, however, sometimes still used as a book–keeping device. At next–to–leading order there are two definitions of Λ that are widely used in the literature:

$$\text{definition 1}: \qquad b \ln \frac{Q^2}{\Lambda^2} = \frac{1}{\alpha_S(\mu^2)} + b' \ln \left(\frac{b' \alpha_S(\mu^2)}{1 + b' \alpha_S(\mu^2)} \right), \tag{6}$$

$$\text{definition 2}: \qquad \alpha_S(\mu^2) = \frac{1}{b \ln(\mu^2/\Lambda^2)} \left[1 - \frac{b'}{b} \frac{\ln \ln(\mu^2/\Lambda^2)}{\ln(\mu^2/\Lambda^2)} \right], \tag{7}$$

where $b' = \beta_1/4\pi\beta_0 = (153 - 19n_f)/(2\pi(33 - 2n_f))$. The first of these solves Eq. (3) exactly when β_2 and higher coefficients are neglected, while the second (the 'PDG' definition [2]) provides an explicit expression for $\alpha_S(\mu^2)$ in terms of μ^2/Λ^2 and is a solution of Eq. (3) up to terms of order $1/\ln^3(\mu^2/\Lambda^2)$.[1] Note that these two Λ parameters are *different* for the *same* value of $\alpha_S(M_Z^2)$, the difference being about one half the size of the current measurement uncertainty:[2]

$$\Lambda_1^{(5)} - \Lambda_2^{(5)} \simeq 15 \text{ MeV} \simeq \frac{1}{2}\delta_{\text{exp}}\Lambda^{(5)}. \tag{8}$$

A second difficulty with the above definitions is that Λ depends on the number of active flavours. Values of Λ for different numbers of flavours can be defined by imposing the continuity of α_S at the scale $\mu = m$, where m is the mass of the heavy quark. For example, for the b-quark threshold: $\alpha_S(m_b^2, 4) = \alpha_S(m_b^2, 5)$. Using the next–to–leading order form (6) for $\alpha_S(\mu^2)$ one can show that

$$\Lambda(4) \approx \Lambda(5) \left(\frac{m_b}{\Lambda(5)} \right)^{\frac{2}{25}} \left[\ln \left(\frac{m_b^2}{\Lambda(5)^2} \right) \right]^{\frac{963}{14375}}. \tag{9}$$

---

[1]The expressions for α_S can be generalized to include also the β_2 term [3].
[2]The latest PDG [2] value is $\Lambda(5) = 212^{+25}_{-23}$ MeV.

Since in practice most higher order QCD corrections are carried out using the $\overline{\text{MS}}$ regularization scheme, one uses either of the above results for $\alpha_S(\mu^2)$ with $\Lambda \equiv \Lambda_{\overline{\text{MS}}}$. Table 2 gives the conversion between $\Lambda_{\overline{\text{MS}}}^{(5)}$ and $\alpha_S(M_Z^2)$ using definition 1 in (6).

Table 2: $\alpha_S(M_Z^2)$ for various $\Lambda_{\overline{\text{MS}}}^{(5)}$.

$\Lambda_{\overline{\text{MS}}}^{(5)}$ (MeV)	$\alpha_S(M_Z^2)$
50	0.0970
100	0.1060
150	0.1122
200	0.1170
250	0.1210
300	0.1245
350	0.1277
400	0.1305
450	0.1332
500	0.1356
550	0.1379
600	0.1401

In these lectures we will be mainly concerned with QCD physics at e^+e^- colliders and in deep inelastic scattering (DIS). Both processes offer several essentially independent measurements of α_S, summarized in Table 3. Note that all of these use the $q\bar{q}g$ vertex to measure α_S, with the high Q^2 scale provided by an electroweak gauge boson, for example a highly virtual γ^* in DIS or an on–shell Z^0 boson at LEP1 and SLC. There are two main theoretical issues that affect these determinations. The first is the effect of unknown higher-order (next–to–next–to–leading order (NNLO) in most cases) perturbative corrections, which leads to a non–negligible renormalisation scheme dependence uncertainty in the extracted α_S values. This is particularly true for the 'event shape' measurements at e^+e^- colliders (see later). The exceptions here are the total e^+e^- hadronic cross section (equivalently, the Z^0 hadronic decay width) and the DIS sum rules, which are known to NNLO. The second issue concerns the residual impact of $\mathcal{O}(1/Q^n)$ power corrections. For some processes it can be shown that the leading corrections are $\mathcal{O}(1/Q)$ (for example $\mathcal{O}(1/M_Z)$ for the corrections to event shapes at LEP1 and SLC) that can easily be comparable in magnitude to the NLO perturbative contributions. In deep inelastic scattering, the higher–twist power corrections to structure functions $F_i(x, Q^2)$ are $\mathcal{O}(1/Q^2(1-x))$ and must be included in scaling violation fits especially at large x. Such power corrections (and their uncertainties) must be taken into account in α_S determinations, either using phenomenological parametrizations or theoretical models.

Figure 1, which updates Table 12.1 of Ref. [1], summarizes the $\alpha_S(M_Z^2)$ measurements from some of the most accurate recent determinations. For experiments performed at energy scales different from M_Z, the α_S values measured at $\mu^2 = Q_{\exp}^2$ are converted to $\alpha_S(M_Z^2)$ using the above expressions. The consistency of the various measurements is remarkable — α_S is indeed a universal parameter. Defining a 'world average' value presents a technical difficulty, however. Since the errors of most of the measurements are largely theoretical — often based on estimates of unknown higher–order corrections or non–perturbative effects — and neither gaussian nor completely independent, the overall error on the combined value of $\alpha_S(M_Z^2)$ cannot be obtained from standard statistical techniques. The average value, obtained

Table 3: Summary of the most important processes for α_S determinations in e^+e^- collisions and in deep inelastic lepton–hadron scattering.

	quantity	perturbation series
e^+e^-	R_{ee}, R_Z, R_τ	$R = R_0[1 + \alpha_S/\pi + \ldots]$
	event shapes, $f_3, \ldots$	$1/\sigma d\sigma/dX = A\alpha_S + B\alpha_S^2 + \ldots$
	$D^h(z, Q^2)$	$\partial D^h/\partial \ln Q^2 = \alpha_S D^h \otimes P + \ldots$
ℓN DIS	$F_i(x, Q^2)$	$\partial F_i/\partial \ln Q^2 = \alpha_S F_i \otimes P + \ldots$
		$\int dx F_i(x, Q^2) = A + B\alpha_S + \ldots$
	$\sigma(2 + 1 \text{ jet})$	$\sigma = A\alpha_S + B\alpha_S^2 + \ldots$

by χ^2 minimisation, of the measurements presented in Fig. 1 is [2]

$$\text{WORLD AVERAGE:} \qquad \alpha_S(M_Z^2) \;=\; 0.1185 \;\pm\; 0.002 \;. \tag{10}$$

The error here is partly a matter of subjective judgement, see the discussions in Refs. [1, 2]. Note that (10) is consistent with, and supercedes, the value of $\alpha_S(M_Z^2) = 0.118 \pm 0.004$ quoted in Ref. [1]. In view of the consistency of all the measurements, and in particular of those with the smallest uncertainties, it seems unlikely that future 'world average' values of α_S will deviate significantly, if at all, from the current value given in (10).

3.   QCD IN HIGH-ENERGY e^+e^- COLLISIONS

Many of the basic ideas and properties of perturbative QCD can be illustrated by considering the process $e^+e^- \to$ hadrons. We begin by discussing how the order α_S corrections to the total hadronic cross section are calculated, and how renormalization scheme dependence enters at order α_S^2. This cross section also provides one of the most precise measurements of the strong coupling, see Fig. 1.

Perturbative QCD also predicts a rich 'jet' structure for the final state hadrons. We show how jet cross sections can be defined, and how some of the predictions compare with experiment.

3.1   The total cross-section for $e^+e^- \to$ hadrons

One of the theoretically most straightforward predictions of perturbative QCD is for $R^{e^+e^-}$, the ratio of the total e^+e^- hadronic cross section to the muon pair production cross section. On the Z^0 pole, as for example at LEP1 and SLC, the analogous quantity is the ratio of the partial decay widths of the Z^0 to hadrons and to muon pairs.

We begin by considering the high–energy $2 \to 2$ process $e^+e^- \to f\bar{f}$ with f a light charged fermion, $f \neq e$. In lowest order, the process is mediated by either a virtual photon or a Z^0 in the s–channel. With θ the centre–of–mass scattering angle of the final state fermion pair, the differential cross section is:

$$\begin{aligned}
\frac{d\sigma}{d\cos\theta} \;=\; \frac{\pi\alpha^2}{2s}\Big[&(1 + \cos^2\theta)\{Q_f^2 - 2Q_f v_e v_f \chi_1(s) \\
&+ (a_e^2 + v_e^2)(a_f^2 + v_f^2)\chi_2(s)\} \\
&+ \cos\theta(-4Q_f a_e a_f \chi_1(s) + 8a_e v_e a_f v_f \chi_2(s))\Big]
\end{aligned} \tag{11}$$

where

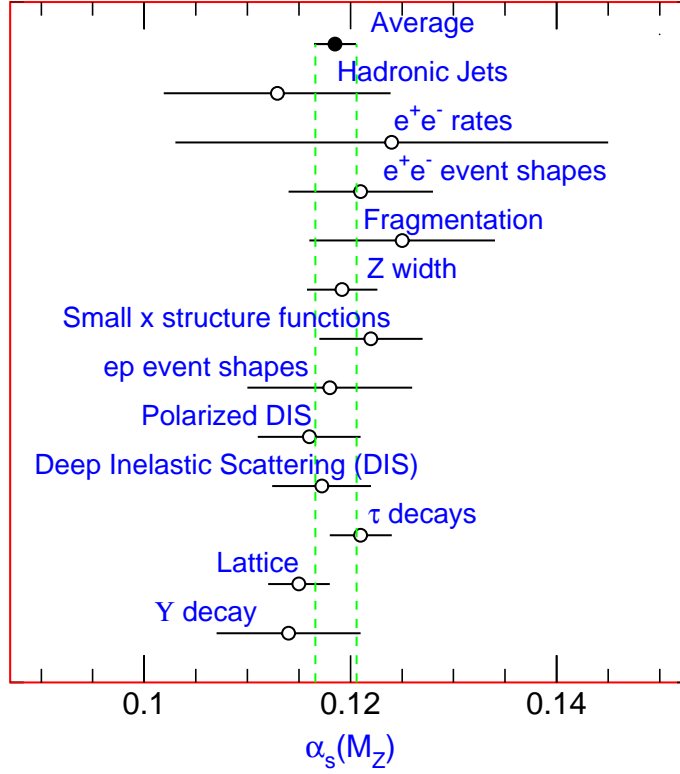$$\chi_1(s) \;=\; \kappa \, \frac{s(s - M_Z^2)}{(s - M_Z^2)^2 + \Gamma_Z^2 M_Z^2}$$

Fig. 1: Measurements of $\alpha_S(M_Z^2)$, in the $\overline{\text{MS}}$ renormalisation scheme, taken from the QCD review in Ref. [2].

$$\chi_2(s) = \kappa^2 \frac{s^2}{(s - M_Z^2)^2 + \Gamma_Z^2 M_Z^2}$$
$$\kappa = \left(\frac{\sqrt{2} G_F M_Z^2}{4\pi\alpha} \right) \tag{12}$$

and (v_f, a_f) are the vector and axial couplings of the fermions to the Z^0.[3] The χ_2 term comes from the square of the Z^0–exchange amplitude and the χ_1 term from the photon–Z^0 interference. Now at centre–of–mass scattering energies $\sqrt{s}$ far below the Z^0 pole, the ratio s/M_Z^2 is small and so $1 \gg \chi_1 \gg \chi_2$. This means that the weak effects — manifest in the terms involving the vector and axial couplings — are quite small and can be neglected. Eq. (11) then reduces to

$$\frac{d\sigma}{d\cos\theta} = \frac{\pi\alpha^2 Q_f^2}{2s}(1 + \cos^2\theta). \tag{13}$$

Integrating over θ and setting $Q_f = -1$ gives the total cross section for $e^+e^- \to \mu^+\mu^-$:

$$\sigma_0 = \frac{4\pi\alpha^2}{3s} \,, \tag{14}$$

where $\sqrt{s}$ is the total centre-of-mass energy. On the Z^0 pole, $\sqrt{s} = M_Z$, the χ_2 term in (11) dominates and the (peak) cross section is

$$\sigma_0 = \frac{4\pi\alpha^2\kappa^2}{3\Gamma_Z^2}(a_e^2 + v_e^2)^2 \,. \tag{15}$$

---

[3] i.e. $v_e = (-1 + 4\sin^2\theta_W)/2$, $a_e = -1/2$ etc.

311

When an electron and a positron annihilate they can also produce hadrons in the final state. The formation of the observed final state hadrons is not governed by perturbation theory. Why then would one expect perturbation theory to give an accurate description of the hadronic production cross section? The answer can be understood by visualizing the event in space–time. The electron and positron form a photon of virtuality $Q = \sqrt{s}$ that fluctuates into a quark and an antiquark. By the uncertainty principle, this fluctuation occurs in a space time volume $1/Q$, and if Q is large the production rate should be predictable in perturbation theory. Subsequently the quarks and gluons form themselves into hadrons. This happens at a later time scale characterized by the scale $1/\Lambda$, where Λ is the typical mass scale of the strong interactions. The interactions that change quarks and gluons into hadrons modify the outgoing state, but they occur too late to modify the probability for an event to happen.

In leading–order perturbation theory, therefore, the total hadronic cross section is obtained by simply summing over all kinematically accessible flavours and colours of quarks. Ignoring the Z^0 exchange contributions (i.e. assuming $\sqrt{s} \ll M_Z$) we have

$$R^{QPM} = \frac{\sum_q \sigma(e^+e^- \to q\bar{q})}{\sigma(e^+e^- \to \mu^+\mu^-)} = 3 \sum_q Q_q^2 \,. \tag{16}$$

With $q = u, ..., b$ we obtain $R^{QPM} = 11/3 = 3.67$. At $\sqrt{s} = 34$ GeV the measured value is about 3.9 (see for example Ref. [2]). Even allowing for the Z^0 contribution ($\Delta R_Z \simeq 0.05$), this result is some 5% higher than the lowest–order prediction. It turns out that the difference is due to higher–order QCD corrections, and in fact the comparison between theory and experiment gives one of the most precise determinations of the strong coupling constant.

The $O(\alpha_S)$ corrections to the total hadronic cross section are calculated from both real and virtual one–gluon emission diagrams. For the real gluon contributions, it is convenient to write the three-body phase space integration as

$$d\Phi_3 \sim d\alpha \; d\beta \; d\gamma \; dx_1 \; dx_2, \tag{17}$$

where α, β, γ are Euler angles, and $x_1 = 2E_q/\sqrt{s}$ and $x_2 = 2E_{\bar{q}}/\sqrt{s}$ are the energy fractions of the final state quark and antiquark. Integrating out the Euler angles gives a matrix element that depends only on x_1 and x_2 and the contribution to the total cross section is

$$\sigma^{q\bar{q}g} = \sigma_0 \, 3 \sum_q Q_q^2 \int dx_1 dx_2 \, \frac{2\alpha_S}{3\pi} \, \frac{x_1^2 + x_2^2}{(1 - x_1)(1 - x_2)} \tag{18}$$

where the integration region is defined by $0 \leq x_1, x_2 \leq 1$, $x_1 + x_2 \geq 1$. Unfortunately, the integrals are divergent at $x_i = 1$! These singularities come from regions of phase space where the gluon is *collinear* with either quark, $\theta_{qg} \to 0$, or where the gluon is *soft*, $E_g \to 0$. Evidently we require some sort of regularization procedure — to render the integrals finite — before the calculation can be completed. A variety of methods are suitable. One can give the gluon a small mass, or take the final state quark and antiquark off–mass–shell by a small amount. In each case the singularities are then manifest as logarithms of the regulating mass.

A more elegant procedure is to use dimensional regularization, with the number of space–time dimensions > 4. With the three–body phase space integrals now cast in n dimensions, the soft and collinear singularities appear as *poles* at $n = 4$. Details of how the calculation proceeds can be found for example in [1]. The result is that the cross section of Eq. (18) becomes

$$\sigma^{q\bar{q}g} = \sigma_0 \, 3 \sum_q Q_q^2 \, \frac{2\alpha_S}{3\pi} \, H(\epsilon) \left[\frac{2}{\epsilon^2} - \frac{3}{\epsilon} + \frac{19}{2} + O(\epsilon) \right], \tag{19}$$

where $\epsilon = (n - 4)/2$ and $H(\epsilon) = 1 + O(\epsilon)$.

The virtual gluon contribution can be calculated in a similar fashion, with dimensional regularization again used to render finite the infra–red divergences in the loops. The result is

$$\sigma^{q\bar{q}(g)} = \sigma_0 \, 3 \sum_q Q_q^2 \, \frac{2\alpha_S}{3\pi} \, H(\epsilon) \left[-\frac{2}{\epsilon^2} + \frac{3}{\epsilon} - 8 + O(\epsilon) \right]. \tag{20}$$

When the two contributions (19) and (20) are added together the poles exactly cancel and the result is *finite* in the limit $\epsilon \to 0$:

$$R^{e^+e^-} = 3 \sum_q Q_q^2 \left\{ 1 + \frac{\alpha_S}{\pi} + O(\alpha_S^2) \right\}. \tag{21}$$

Note that the next-to-leading order correction is positive, and with a value for α_S of about 0.15, can accommodate the experimental measurement at $\sqrt{s} = 34$ GeV.[4]

The cancellation of the soft and collinear singularities between the real and virtual gluon diagrams is not accidental. Indeed, there are theorems — the Bloch, Nordsieck [4] and Kinoshita, Lee, Nauenberg [5] theorems — which state that suitably defined inclusive quantities will be free of singularities in the massless limit. The total hadronic cross section is an example of such a quantity, whereas the cross section for the exclusive $q\bar{q}$ final state, i.e. $\sigma(e^+e^- \to q\bar{q})$, is not.

The $O(\alpha_S^2)$ and $O(\alpha_S^3)$ corrections to $R^{e^+e^-}$ are also known. At these higher orders we encounter the ultra–violet divergences associated with the renormalization of the strong coupling. Writing

$$\sigma_{tot} = \frac{4\pi\alpha^2}{3s} R,$$
$$R = K_{QCD} \, 3 \sum_q Q_q^2,$$
$$K_{QCD} = 1 + \sum_{n \geq 1} C_n \left(\frac{\alpha_S}{\pi} \right)^n , \tag{22}$$

the coefficients C_1, C_2 and C_3 are (in the $\overline{\text{MS}}$ scheme with the renormalization scale choice $\mu = \sqrt{s}$):

$$C_1 = 1$$
$$C_2 = \left(\frac{2}{3}\zeta(3) - \frac{11}{12} \right) n_f + \left(\frac{365}{24} - 11\zeta(3) \right)$$
$$\simeq 1.986 - 0.115 n_f$$
$$C_3 = \left(\frac{87029}{288} - \frac{1103}{4}\zeta(3) + \frac{275}{6}\zeta(5) \right)$$
$$- \left(\frac{7847}{216} - \frac{262}{9}\zeta(3) + \frac{25}{9}\zeta(5) \right) n_f$$
$$+ \left(\frac{151}{162} - \frac{19}{27}\zeta(3) \right) n_f^2$$
$$- \frac{\pi^2}{432}(33 - 2n_f)^2 + \eta \left(\frac{55}{72} - \frac{5}{3}\zeta(3) \right)$$
$$\simeq -6.637 - 1.200 n_f - 0.005 n_f^2 - 1.240 \eta , \tag{23}$$

where $\eta = (\sum_q Q_q)^2 / (3 \sum_q Q_q^2)$ and the sum extends over the (n_f) quarks that are effectively massless at the energy scale $\sqrt{s}$. The result for C_3 is from Ref. [6]. Apart from the η term, the QCD corrections in K are the same for the ratio of hadronic to leptonic Z^0 decay widths: $R_Z = \Gamma_h/\Gamma_\mu$. In practice, quark masses (particularly m_b and m_t) have a small but non–negligible effect [7] and must be taken into account in precision fits to data.

---

[4]In contrast, the corresponding correction is negative for a scalar gluon.

Experiments at LEP1 and SLC were able to measure R_Z very accurately. From such measurements, a very precise value of $\alpha_S(M_Z^2)$ can be obtained. In practice, α_S is measured simultaneously with other parameters in a global electroweak fit, and the value obtained is correlated to some extent with m_t, M_H, etc. A recent fit of this kind [8] gives

$$\alpha_S(M_Z^2) = 0.118 \pm 0.003, \tag{24}$$

in excellent agreement with the world average value (10).

Through $\mathcal{O}(\alpha_S^3)$, the explicit μ–dependence of the perturbation series for R is restored by the replacements:

$$
\begin{aligned}
\alpha_S & \rightarrow \alpha_S(\mu^2) \\
C_2 & \rightarrow C_2 - C_1 \frac{\beta_0}{4} \log \frac{s}{\mu^2} \\
C_3 & \rightarrow C_3 + C_1 \left(\frac{\beta_0}{4}\right)^2 \log^2 \frac{s}{\mu^2} - (C_1 \frac{\beta_1}{16} + C_2 \frac{\beta_0}{2}) \log \frac{s}{\mu^2}.
\end{aligned}
\tag{25}
$$

where β_0 and β_1 have been defined in Section 2 above. Note that the μ^2–dependence of the second order coefficient is exactly as specified by the renormalization group equation, i.e. the coefficient of $\log(s/\mu^2)$ is proportional to the β function coefficient defined in (3).

In general the coefficients of any QCD perturbative expansion depend on the choice made for the renormalization scale μ in such a way that as μ is varied, the change in the coefficients exactly compensates the change in the coupling $\alpha_S(\mu^2)$. However this μ–independence breaks down whenever the series is *truncated*. One can show in fact that changing the scale in a physical quantity such as $R^{e^+e^-}$ — which has been calculated to $O(\alpha_S^n)$ — induces changes of $O(\alpha_S^{n+1})$. This is illustrated in Fig. 2, taken from Ref. [1], which shows $K_{QCD} = 1 + \delta$ for R_Z as a function of μ, as the higher–order terms are added in.
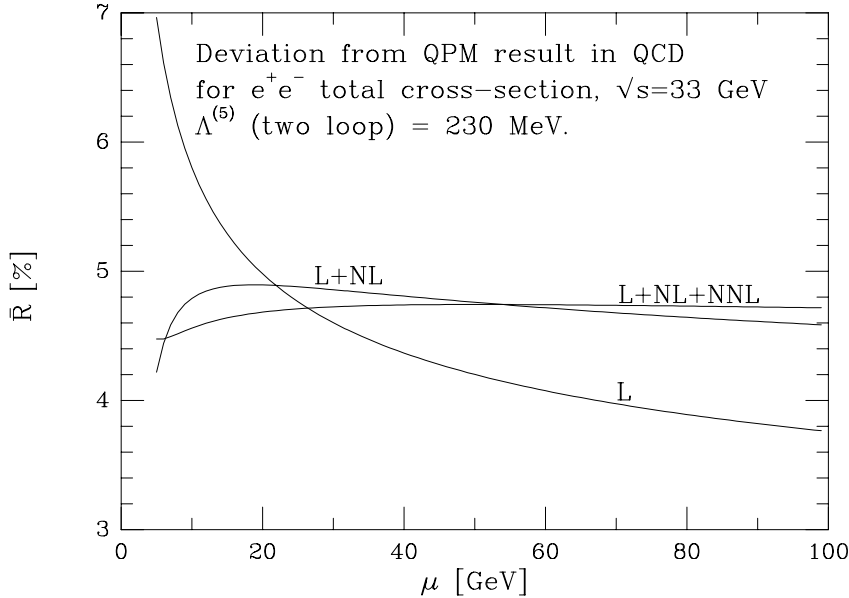

Fig. 2: The effect of higher order QCD corrections to R_Z, as a function of the renormalization scale μ, from Ref. [1].

As expected, the inclusion of higher–order terms leads to a more definite prediction. In the absence of higher–order corrections, one can try to guess the 'best' choice of scale, defined as the scale that makes the truncated and all–orders predictions equal. In the literature, two such choices have been advocated in particular. In the *fastest apparent convergence* approach [9], one chooses the scale $\mu = \mu_{\mathrm{FAC}}$, where

$$R^{(1)}(\mu_{\mathrm{FAC}}) = R^{(2)}(\mu_{\mathrm{FAC}}). \tag{26}$$

On the other hand, the *principle of minimal sensitivity* [10] suggests a scale choice $\mu = \mu_{\mathrm{PMS}}$, where

$$\mu \frac{\mathrm{d}}{\mathrm{d}\mu} R^{(2)}(\mu)\Big|_{\mu_{\mathrm{PMS}}} = 0. \tag{27}$$

These two special scales can be identified in Fig. 2. It is, however, important to remember that there are no theorems that prove that any of these schemes are correct. All one can say is that the theoretical error on a quantity calculated to $O(\alpha_S^n)$ is $O(\alpha_S^{n+1})$. Varying the scale is simply one way of quantifying this uncertainty.

3.2 Jet cross-sections

The expression given for the total hadronic cross section in the previous section is very concise, but it tells us nothing about the kinematic *distribution* of hadrons in the final state. If the hadronic fragments of a fast moving quark have limited transverse momentum relative to the quark momentum, then the lowest order contribution — $e^+e^- \to q\bar{q}$ — can naively be interpreted as the production of two back–to–back jets. In this section we investigate how higher–order perturbative corrections modify this picture.

Consider first the next–to–leading process $e^+e^- \to q\bar{q}g$. From the previous section (Eq. (18)), we have

$$\frac{1}{\sigma}\frac{\mathrm{d}^2\sigma}{\mathrm{d}x_1\mathrm{d}x_2} = \frac{2\alpha_S}{3\pi}\frac{x_1^2 + x_2^2}{(1-x_1)(1-x_2)} . \tag{28}$$

Recall that the cross section becomes infinitely large when either (a) the gluon is collinear with one of the outgoing quarks, or (b) the gluon momentum goes to zero. This corresponds to (a) only one and (b) both of the x_i approaching 1 respectively. In other words the gluon prefers to be soft and/or collinear with the quarks. If the gluon is *required* to be well–separated in phase space from the quarks — a configuration corresponding to a 'three jet event' — then the cross section is suppressed relative to lowest order by one power of α_S. It would appear, therefore, that the two–jet nature of the final state is maintained at next–to–leading order, since both the preferred configurations give a final state indistinguishable (after parton fragmentation to hadrons) from that at lowest order. This qualitative result holds in fact to *all* orders of perturbation theory. Multigluon emission leads to a final state that is predominantly 'two–jet–like', with a smaller probability (determined by α_S) for three or more distinguishable jets.

To quantify this statement we need to introduce the concept of a *jet measure*, i.e. a procedure for classifying a final state of hadrons (experimentally) or quarks and gluons (theoretically) according to the number of jets. To be useful, a jet measure should be free of soft and collinear singularities when calculated in perturbative QCD, and should also be relatively insensitive to the non–perturbative fragmentation of quarks and gluons into hadrons.

One of the most widely used jet measures is the 'minimum invariant mass' or JADE algorithm [11]. Consider a $q\bar{q}g$ final state. A three–jet event is one in which the invariant masses of the parton pairs are all larger than some fixed fraction y of the overall centre–of–mass energy:

$$(p_i + p_j)^2 > ys, \qquad i,j = q,\bar{q},g. \tag{29}$$

It is immediately clear that this region of phase space avoids the soft and collinear singularities of the matrix element. In fact in terms of the energy fractions, Eq. (29) is equivalent to

$$0 < x_1, x_2 < 1 - y, \qquad x_1 + x_2 > 1 + y. \tag{30}$$

If we define f_2 and f_3 to be the two– and three–jet fractions defined in this way, then to $O(\alpha_S)$ we obtain

$$f_3 = \frac{2\alpha_S}{3\pi}\left[(3-6y)\log\left(\frac{y}{1-2y}\right) + 2\log^2\left(\frac{y}{1-y}\right) + \frac{5}{2} - 6y - \frac{9}{2}y^2\right.$$
$$\left. + 4\,\mathrm{Li}_2\left(\frac{y}{1-y}\right) - \frac{\pi^2}{3}\right], \quad \mathrm{Li}_2(y) = -\int_0^y \frac{\mathrm{d}z}{1-z}\log z\,,$$
$$f_2 = 1 - f_3\,. \tag{31}$$

Note that the soft and collinear singularities reappear as large logarithms in the limit $y \to 0$. Clearly the result only makes sense for y values large enough such that $f_2 \gg f_3$, so that the $O(\alpha_S)$ correction to f_2 is perturbatively small.

The generalization to multijet fractions is straightforward. Starting from an n–parton final state, identify the pair with the minimum invariant mass squared. If this is greater then ys then the number of jets is n. If not, combine the minimum pair into a single 'cluster'. Then repeat for the $(n-1)$–parton/cluster final state, and so on until all parton/clusters have a relative invariant mass squared greater than ys. The number of clusters remaining is then the number of jets in the final state. Note that an n–parton final state can give any number of jets between n (all partons well-separated) and 2 (for example, two hard quarks accompanied by soft and collinear gluons).

Since a soft or collinear gluon emitted from a quark line does not change the multiplicity of jets, the cancellation of soft and collinear singularities that was evident in the total cross section calculation can still take place, and the jet fractions defined this way are free of such singularities to all orders in perturbation theory.

Now in general we have

$$f_{n+2}(\sqrt{s}, y) = \left(\frac{\alpha_S(s)}{\pi}\right)^n \sum_{j=0}^{\infty} C_{nj}(y)\left(\frac{\alpha_S(s)}{\pi}\right)^j, \quad n \geq 0,$$
$$\sum_{n=2}^{\infty} f_n = 1\,. \tag{32}$$

Since the jet–defining parameter y is dimensionless, all the energy dependence of the jet fractions is contained in the coupling $\alpha_S(s)$. One can therefore exhibit the *running* of the strong coupling by measuring a decrease in f_3 as $\sqrt{s}$ increases, see Fig. 3. Note that experimentally the algorithm is applied to final state *hadrons* rather than *partons*. However studies using parton shower/fragmentation Monte Carlos have shown that — at least at very high energy — the fragmentation corrections are small ($\mathcal{O}(1/Q)$, see Section 3.4 below) and therefore the QCD parton–level predictions can be reliably compared with the experimental data. A quantitative discussion can be found in Ref. [15], for example.

The next–to–leading order corrections to f_3 have been calculated [12]. Because the hadronization corrections to f_3 are relatively small, the three–jet rate provides one of the most precise measurements of α_S at LEP and SLC. A typical fit is shown in Fig. 4.

While the above definition is well suited to experimental jet measurements, it is not quite optimum from a theoretical point of view. The reason is that when y becomes small (as happens in practice), the large logarithms of y explicit in (31) begin to dominate the theoretical predictions. It is straightforward to show that higher–order corrections to jet fractions such as f_2 and f_3 will contain terms like $\alpha_S^n \log^{2n} y$. When y is small enough that $\alpha_S \log^2 y \sim 1$, these terms must be resummed to obtain a reliable prediction. Unfortunately, the JADE algorithm is not well-suited to this type of resummation [16], and so a variant — the 'Durham' or k_T algorithm —- was proposed [17]. In this modified algorithm, the invariant mass measure of two partons (hadrons) given in (29) is replaced by the minimum of the relative transverse momenta:

$$\min k_{Tij}^2 = \min(E_i^2, E_j^2)\sin\theta_{ij}^2 > ys, \quad i, j = q, \bar{q}, g\,, \tag{33}$$
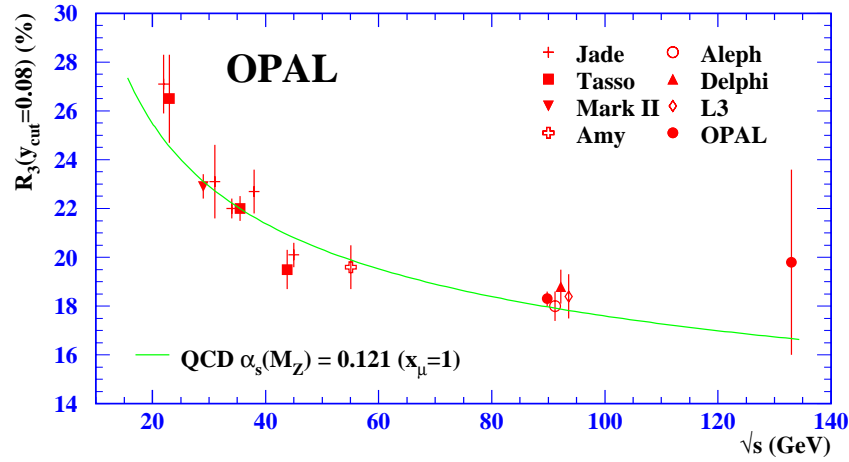
316

Fig. 3: A compilation of three-jet fractions (R_3) at different e^+e^- annihilation energies, from the OPAL collaboration [13].
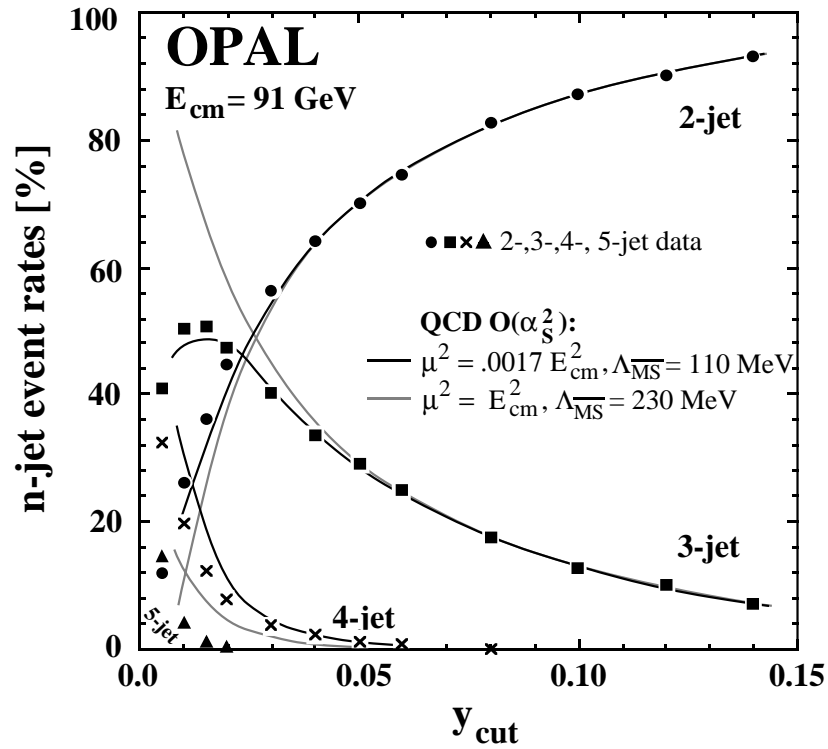

Fig. 4: Multijet rates measured by the OPAL collaboration [14], with perturbative QCD fits.

in the e^+e^- centre–of–mass frame with massless quarks and gluons. With this new definition of the jet measure, resummation of all large logarithms can be performed [17]. Finite, next–to–leading order corrections have also been calculated [15] and comparisons of theory and experiment have been performed, as for the JADE algorithm. It is interesting that the (presumably) more reliable α_S values from resummed perturbative jet measures tend to be slightly larger than those obtained without resummation, see for example Table 12.1 in Ref. [1].

3.3 Event shape variables

The other high–precision determination of α_S at LEP and SLC comes from *event shape* variables, quantities that characterize the 'shape' of an event, for example whether the distribution of hadrons is pencil–like, planar, spherical etc. This is more general than the jet cross section approach discussed above, since a jet-finding algorithm will *always* find jets in a hadronic final state even when none existed in the first place, for example in the limiting case when the hadronic energy is distributed uniformly over the 4π solid angle. The procedure is to define a quantity X that measures some particular aspect of the shape of the hadronic final states. The distribution $d\sigma/dX$ can be measured and compared with the theoretical prediction. For the latter to be calculable in perturbation theory, the variable should be infra–red safe, i.e. insensitive to the emission of soft or collinear gluons. A typical example is the thrust variable:

$$T = \max_{\mathbf{n}} \frac{\sum_i |\mathbf{p_i} \cdot \mathbf{n}|}{\sum_i |\mathbf{p_i}|}. \tag{34}$$

Thus a pure two–particle final state (e.g. $q\bar{q}$) has $T = 1$, while for $T < 1$ the leading order (parton) contribution to the thrust distribution comes from the $q\bar{q}g$ final state:

$$\frac{1}{\sigma} \frac{d\sigma}{dT} = \alpha_S A_1(T) + \alpha_S^2 A_2(T) + \ldots + \mathcal{O}\left(\frac{1}{E_{\text{cm}}}\right), \tag{35}$$

where the coefficient functions $A_1(T)$ and $A_2(T)$ have been calculated. Thus the *shape* of the distribution tests, via $A_1(T)$, the basic QCD $q\bar{q}g$ interaction vertex (scalar gluons would, for example, give a different shape and can be excluded by the data), while the overall normalization provides a measure of α_S. At present, quantities like the thrust distribution are known in perturbation theory to $\mathcal{O}(\alpha_S^2)$, and the theoretical predictions in the $T \to 1$ region can be improved by resumming the leading logarithmic $A_n \sim \ln^{(2n-1)}(1-T)/(1-T)$ contributions to all orders. This yields a 'Sudakov' form factor:

$$\frac{1}{\sigma} \frac{d\sigma}{dT} \sim \frac{\partial}{\partial T} \exp(-\alpha_S C_F/\pi \ln^2(1-T)). \tag{36}$$

Evidently the dominant effect of resummation is to suppress the event fraction at $T \approx 1$, leading to a turn-over instead of a divergence in the distribution at high thrust. It can be shown, however, that in the vicinity of the turn-over the double leading logarithm approximation is not reliable, and sub-leading logarithms at each order have to be taken into account (see the discussion in Ref. [1], for example). When this is done, and when the resummed predictions are matched to the exact NNLO contribution (i.e. the full $A_1(T)$ and $A_2(T)$) excellent agreement with experiment is obtained, see Fig. 5. Another important recent theoretical development, discussed in the following section, has been an improved understanding of the leading $\mathcal{O}(1/E)$ power corrections, which at LEP can be as numerically important as the next–to–leading perturbative corrections.

Event shapes have yielded α_S measurements over a wide range of e^+e^- collision energies, the most recent measurements being at LEP2 up to $\sqrt{s} = \mathcal{O}(200 \text{ GeV})$. Although the statistical precision of these measurements cannot match that obtained at the Z^0 pole, the results are consistent with the Q^2 evolution of α_S predicted by Eq. (3). For example, Fig. 6 shows the α_S values determined by the L3 collaboration [19] from event shape measurements at LEP1 and LEP2 energies. The solid line is the evolution predicted by perturbative QCD.
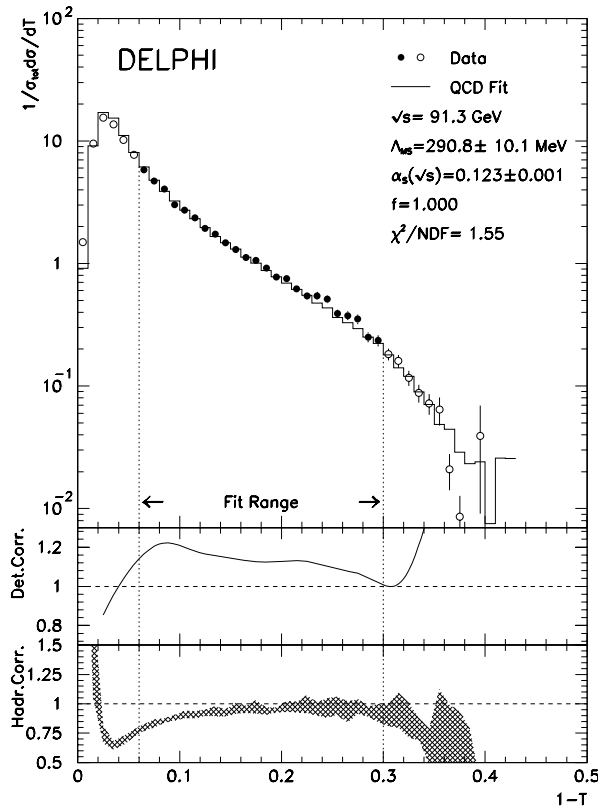
Fig. 5: Resummed prediction for the thrust distribution at LEP, corrected for hadronisation and fitted to DELPHI data, from Ref. [18].

3.4 Power corrections

Event shape variables in $e^+e^-, ep, \ldots$ collisions provide powerful tests of perturbative QCD. A recent development has been the realisation that certain nonperturbative *power corrections* may be universal [20, 21, 22]. If this is indeed true, it will sharpen the phenomenology and improve the determinations of α_S. In general, the average value of a shape variable X can be written as

$$\langle X \rangle = \alpha_S A_1 + \alpha_S^2 A_2 + \ldots \quad + O\left(\frac{1}{Q^n}\right) \qquad (n \geq 1), \tag{37}$$

where the perturbative A_i coefficients can be computed to arbitrary order, at least in principle. The scale for the power corrections is expected to be $\mathcal{O}(1 \text{ GeV})$, at least for quantities dominated by light quarks and gluons, and so $n = 1$ power corrections can easily contribute at the same level as $\mathcal{O}(\alpha_S^2)$ perturbative corrections. In fact it is well known that 'hadronisation' corrections to event shapes in e^+e^- annihilation, as modelled by Monte Carlos such as HERWIG and JETSET, do indeed exhibit a $1/Q$ dependence and need to be taken into account in α_S determinations such as those described above.

To see how universal power corrections might arise, consider the calculation of the average of an event shape variable at leading order in perturbation theory. The average is given by a phase-space integral over the $q\bar{q}g$ matrix element squared, weighted by an appropriate quantity-dependent factor that guarantees infra-red safety; schematically,

$$
\begin{aligned}
\langle X \rangle &= \int d[k, \ldots] \, |\mathcal{M}_{q\bar{q}g}|^2 \, \mathcal{W}_X(k) \; + \; \ldots \\
&\sim \int_0^Q \frac{dk}{k} \left\{ a_X \left(\frac{k}{Q}\right)^p \alpha_S(k^2) + \ldots \right\} \\
&\sim \int_{\mu_I}^Q \frac{dk}{k} \{\ldots\} \; + \; a_X \left(\frac{\mu_I}{Q}\right)^p \int_0^{\mu_I} \frac{dk}{k} \left(\frac{k}{\mu_I}\right)^p \alpha_S(k^2),
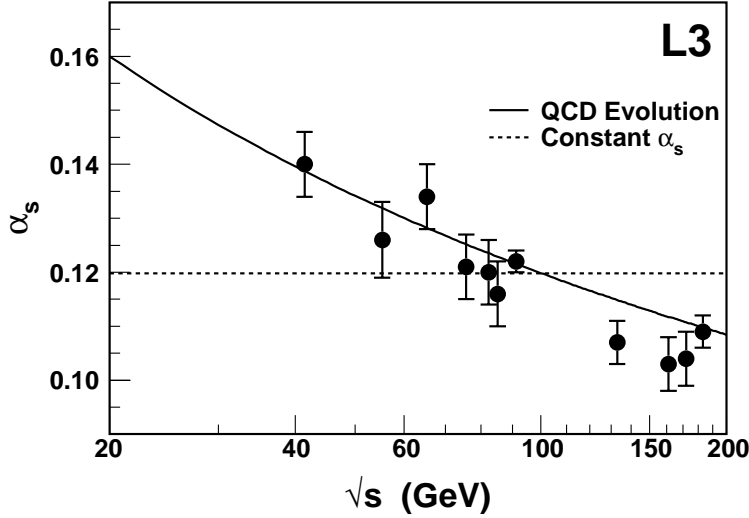\end{aligned}
\tag{38}
$$

319

Fig. 6: Measurements of α_S from event shapes at LEP1 and LEP2 from the L3 collaboration [19]. The errors correspond to experimental uncertainties only.

where k is the energy of the emitted gluon. In the second step the behaviour at small k is exposed, and in the last step we have split the integral over the gluon energy into a part $k > \mu_I$ for which $\alpha_S \ll 1$ and for which perturbation theory applies, and a part $k < \mu_I$ for which the coupling is large and its precise form unknown. The strength of the infra-red suppression p depends on the quantity X. We may define a non-perturbative parameter to represent the contribution from the $k < \mu_I$ region:

$$\overline{\alpha}_{p-1}(\mu_I) = \int_0^{\mu_I} \frac{dk}{k} \left(\frac{k}{\mu_I} \right)^p \alpha_S(k^2). \tag{39}$$

Consider, for example, the average thrust $\langle T \rangle$ in e^+e^- annihilation. Explicit calculation gives $p = 1$, $a_T = -4C_F/\pi$. A fit to the experimental data using NLO perturbation theory and a $1/Q$ power correction supplemented by the so-called Milan factor[5] ($= 1.8$) gives a very good description, and yields a value for the parameter $\overline{\alpha}_0(\mu_I)$ at a particular reference scale. For example [23]

$$\langle 1 - T \rangle : \qquad \overline{\alpha}_0(2 \text{ GeV}) \quad = \quad 0.493 \pm 0.009 \pm 0.004, \tag{40}$$

where the second error is from the scale variation $E/2 \to 2E$. The formalism can also be extended to *distributions* in the shape variables, e.g. $d\sigma/dT$, see for example Ref. [22].

A powerful check on the above method of quantifying the leading power corrections is to see whether the parameter $\overline{\alpha}_p$ is indeed universal. Recently the formalism has also been applied to shape variables measured in ep collisions at HERA. The result of a fit to a variety of variables by the H1 collaboration is shown in Fig. 7. The agreement with the e^+e^- values of Eq. (40) is reasonable, although not perfect. This could be evidence for non-negligible subleading power corrections in one or other process. In any case, the formalism described above represents a major advance in our quantitative understanding of power corrections. As for α_S measurements, one could hope to compile a set of $\overline{\alpha}_0, \overline{\alpha}_1, \ldots$ parameters measured in a variety processes to check for universal behaviour.

There are many other detailed tests of QCD that can be performed at high–energy e^+e^- colliders, but lack of space precludes a detailed discussion here. Some of most important are: (i) using four–jet events to test the non–Abelian strucure of QCD via the $e^+e^- \to q\bar{q}gg$ process, (ii) studying the detailed

---

[5]The effect of soft gluons on the nonperturbative contribution at the two-loop level has been analysed by Dokshitzer *et al.* [24], and shown to yield an additional enhancement 'Milan' factor.
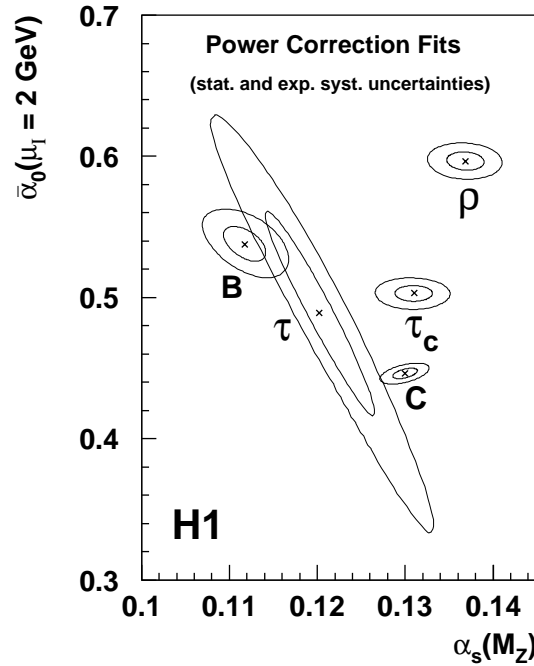
Fig. 7: Simultaneous measurements of α_S and the non-perturbative power-correction parameter $\overline{\alpha}_0$ by the H1 collaboration [25].

structure of (light and heavy) quark jets and gluon jets, (iii) comparing measured particle multiplicities with leading-logarithm ('MLLA') QCD predictions. Further information can be found in Ref. [1].

4. DEEP INELASTIC SCATTERING

The original, and still one of the the most powerful, test of perturbative QCD is the breaking of Bjorken scaling in the structure functions measured in deep inelastic lepton–hadron scattering. Nowadays, structure function analyses not only provide some of the most precise tests of the theory but also determine the momentum distributions of partons in hadrons for use as input in predicting cross sections in high energy hadron–hadron collisions. In this section we first describe the basic features of the parton model in deep inelastic scattering and then discuss how the picture is modified by perturbative corrections. Comprehensive reviews of deep inelastic scattering, the parton model and QCD can be found in Refs. [1] and [26], for example.

4.1 The parton model

Consider the deep inelastic lepton–proton scattering process $lp \to lX$. Label the incoming and outgoing lepton four–momenta by k^μ and k'^μ respectively, the incoming proton momentum by p^μ ($p^2 = M^2$) and the momentum transfer by $q^\mu = k^\mu - k'^\mu$. The standard deep inelastic variables are defined by:

$$
\begin{aligned}
Q^2 &= -q^2 \qquad p^2 = M^2 \\
x &= \frac{Q^2}{2p \cdot q} = \frac{Q^2}{2M(E - E')} \\
y &= \frac{q \cdot p}{k \cdot p} = 1 - E'/E \\
s &= (k + p)^2 = M^2 + \frac{Q^2}{xy},
\end{aligned}
\tag{41}
$$

where the energies are defined in the rest frame of the target. Analogous expressions can be derived for lepton–hadron *colliders*, such as HERA. The hadronic structure functions $F_i(x, Q^2)$ are then defined in terms of the inclusive lepton scattering cross sections. For example, for charged lepton (neutral current) scattering via virtual photon exchange, $lp \to lX$,

$$
\frac{d^2\sigma^{em}}{dxdy} = \frac{4\pi\alpha^2(s - M^2)}{Q^4}\left[\left(\frac{1 + (1 - y)^2}{2}\right)2xF_1^{em}\right.
$$
$$
\left. +(1 - y)(F_2^{em} - 2xF_1^{em}) - \frac{M^2}{s - M^2}xyF_2^{em}\right], \tag{42}
$$

and for neutrino or antineutrino (charged current) scattering via virtual W exchange, $\nu(\bar{\nu})p \to lX$,

$$
\frac{d^2\sigma^{\nu(\bar{\nu})}}{dxdy} = \frac{G_F^2(s - M^2)}{2\pi}\left[\left(1 - y - \frac{M^2}{s - M^2}xy\right)F_2^{\nu(\bar{\nu})}\right.
$$
$$
\left. +y^2xF_1^{\nu(\bar{\nu})} + (-)y(1 - y/2)xF_3^{\nu(\bar{\nu})}\right]. \tag{43}
$$

In the quark–parton model, these structure functions are related to the quark 'distribution functions' or 'densities' $q(x, \mu^2)$, where $q(x, \mu^2)dx$ is the probability that a quark parton q carries a momentum fraction x of the target nucleon's momentum when probed (by a gauge boson γ^*, W or Z) at momentum transfer scale μ. In deep inelastic scattering the relevant scale is the virtuality of the gauge boson probe, i.e. $\mu^2 = Q^2$. Thus, assuming four approximately massless quark flavours,

$$
\begin{aligned}
F_2^\nu &= 2x[d + s + \bar{u} + \bar{c}] \\
xF_3^\nu &= 2x[d + s - \bar{u} - \bar{c}] \\
F_2^{\bar{\nu}} &= 2x[u + c + \bar{d} + \bar{s}] \\
xF_3^{\bar{\nu}} &= 2x[u + c - \bar{d} - \bar{s}] \\
F_2^{em} &= x\left[\frac{4}{9}(u + u + c + \bar{c}) + \frac{1}{9}(d + \bar{d} + s + \bar{s})\right] \\
F_L \equiv F_2 - 2xF_1 &= 0. \tag{44}
\end{aligned}
$$

This last result, the vanishing of the structure function for longitudinal virtual photon scattering, is called the Callan–Gross relation and follows from the spin$-1/2$ property of the quarks. Note that when the nature of the target is unambiguous, the notation $q(x, \mu^2)$ and $g(x, \mu^2)$ for the quark and gluon densities can be used, otherwise a general notation is $f_{a/A}(x, \mu^2)$, where a = u, d, ... g and A = p, n, Fe, Cu, etc. In the 'naive' parton model the structure functions *scale*, i.e. $F(x, Q^2) \to F(x)$ in the asymptotic (Bjorken) limit: $Q^2 \to \infty$, x fixed. In fact, it was the observation of scaling in the original SLAC experiments that provided the first evidence of pointlike parton structure in the hadron. To a first approximation, therefore, one can take the parton distributions to be functions of x only: $q(x, \mu^2) \to q(x)$. We shall see below how perturbative QCD induces logarithmic deviations from scaling, exactly in line with more recent high–precision experimental measurements.

Individual quark distributions can be determined from measurements of the various structure functions in (44). A picture emerges in which a proton consists of three valence quarks (uud) and a 'sea' of $q\bar{q}$ pairs and gluons. In the most simple version of this parton model the sea would be (three) flavour symmetric and hence the net quark distributions would be given by $u = u_V + S$, $d = d_V + S$ and $s = \bar{s} = \bar{u} = \bar{d} = S$, with the sum rules

$$
\int_0^1 u_V(x)dx = 2\int_0^1 d_V(x)dx = 2, \tag{45}
$$

$$
\int_0^1 x[u_V(x) + d_V(x) + 6S(x)]dx = 1. \tag{46}
$$

322

These represent conservation of proton quantum numbers and total momentum fraction respectively.
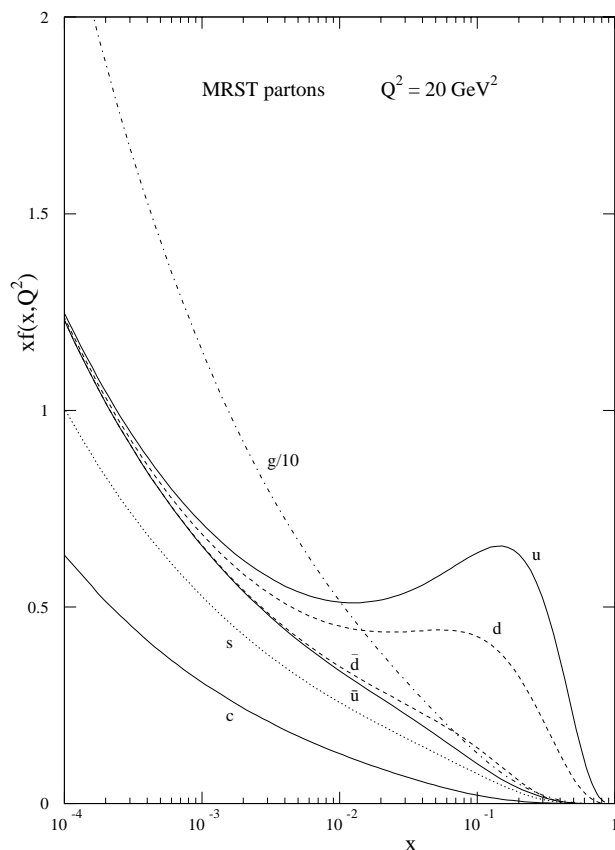

Fig. 8: Quark and gluon distribution functions at $\mu^2 = 20$ GeV^2, from Ref. [27].

Figure 8 shows a typical set of 'modern' quark and gluon distributions $xf_i(x, \mu^2)$ [27] in the proton extracted from fits to deep inelastic and other data, when probed at a momentum scale $\mu^2 = 20$ GeV^2, a typical value for fixed–target deep inelastic experiments. Notice that the sea is definitely *not* SU(3) flavour symmetric, rather the strange quark distribution is roughly a factor of 2 smaller than the light sea quarks, and there is even a significant asymmetry between the $\bar{u}$ and $\bar{d}$ quarks in the sea. Neither of these features is quantitatively understood at present. Qualitatively, one would expect smaller distributions for heavier sea quarks, i.e. $\bar{u}, \bar{d} > s > c > b > \ldots$, and some sort of Fermi exclusion principle ($u > d \Rightarrow \bar{u} < \bar{d}$) might explain the asymmetry between $\bar{u}$ and $\bar{d}$. Notice also that at this scale a small charm quark component *is* observed, consistent with the expectation that the virtual photon should be able to resolve $c\bar{c}$ pairs in the quark sea when $Q^2 > O(m_c^2)$. The sum rule (45) is experimentally well verified, but the net momentum fraction (46) carried by the quarks alone is found to be only about 50%, with the gluons (not directly measured in leading–order deep inelastic scattering, see below) accounting for the other 50%.

4.2 Scaling violations – the DGLAP evolution equations

In QCD, Bjorken scaling is broken by logarithms of Q^2. Physically, a quark in the proton can emit a gluon, with probability determined by α_S, and lose momentum as a result. Since the higher the Q^2 the more phase space is available for gluon emission, the expectation is that parton distributions should shrink to small x as Q^2 increases, with the rate of shrinkage being controlled by α_S.

In describing quantitatively the way in which scaling is violated it is convenient to define singlet and non–singlet quark distributions:

$$
\begin{aligned}
F^{NS}(x, Q^2) &= q_i(x, Q^2) - q_j(x, Q^2) \,, \\
F^S(x, Q^2) &= \sum_i \left[q_i(x, Q^2) + \bar{q}_i(x, Q^2) \right] \,,
\end{aligned}
\tag{47}
$$

where we have restored the explicit Q^2 dependence. The non–singlet structure functions have non–zero values of flavour quantum numbers such as isospin or baryon number. The variation with Q^2 of these functions is described by the Dokshitzer–Gribov–Lipatov–Altarelli–Parisi (DGLAP) equations [28]:

$$
\begin{aligned}
Q^2 \frac{\partial F^{NS}}{\partial Q^2} &= \frac{\alpha_S(Q^2)}{2\pi} P^{qq} * F^{NS} \\
Q^2 \frac{\partial F^S}{\partial Q^2} &= \frac{\alpha_S(Q^2)}{2\pi} \left(P^{qq} * F^S + 2n_f P^{qg} * g \right) \\
Q^2 \frac{\partial g}{\partial Q^2} &= \frac{\alpha_S(Q^2)}{2\pi} \left(P^{gq} * F^S + P^{gg} * g \right),
\end{aligned}
\tag{48}
$$

where $*$ denotes a convolution integral:

$$
f * g = \int_x^1 \frac{dy}{y} f(y) g\left(\frac{x}{y}\right).
\tag{49}
$$

In leading order the DGLAP kernels (or 'splitting functions') are

$$
\begin{aligned}
P^{qq} &= \frac{4}{3} \left(\frac{1 + x^2}{1 - x} \right)_+ \\
P^{qg} &= \frac{1}{2} \left[x^2 + (1 - x)^2 \right] \\
P^{gq} &= \frac{4}{3} \left[\frac{1 + (1 - x)^2}{x} \right] \\
P^{gg} &= 6 \left[\frac{1 - x}{x} + x(1 - x) + \left(\frac{x}{1 - x} \right)_+ \right] \\
&\quad - \left[\frac{1}{2} + \frac{n_f}{3} \right] \delta(1 - x).
\end{aligned}
\tag{50}
$$

Note the 'plus prescription' for those functions that are singular as $x \to 1$:

$$
\int_0^1 dx f(x) \left(g(x) \right)_+ = \int_0^1 dx [f(x) - f(1)] g(x).
\tag{51}
$$

The DGLAP equations can be solved analytically by defining $moments$ (formally, Mellin transforms) of the structure functions, $M_n^{NS} = \langle F^{NS} \rangle_n \equiv \int_0^1 dx x^{n-1} F^{NS}$ etc. The convolution integral then becomes a simple product. Introducing the leading–order expression for the QCD coupling constant derived in Section 2.2,

$$
\alpha_S(Q^2) = \frac{4\pi}{\beta_0 \ln(Q^2/\Lambda^2)},
\tag{52}
$$

one obtains, for the non–singlet solution,

$$M_n^{NS}(Q^2) = M_n^{NS}(Q_0^2) \left(\frac{\alpha_S(Q^2)}{\alpha_S(Q_0^2)} \right)^{-d_n}, \qquad (53)$$

where $d_n = 2\langle P^{qq} \rangle_n / \beta_0$. Note that $d_1 = 0$ and that $d_n < 0$ for $n \geq 2$, which implies that the parton distributions decrease and increase with increasing Q^2 at large and small x respectively, as argued on physical grounds above. Solutions for the singlet and gluon moments can be found in a similar way, by first diagonalizing the coupled equations. In practice, it is often more convenient to solve the DGLAP equations numerically by iterating small steps in $\log Q^2$, starting from a set of 'input' parton distributions $f_i(x, Q_0^2)$. Figure 9 shows the same set of parton distribution functions as in Fig. 8, but now DGLAP–
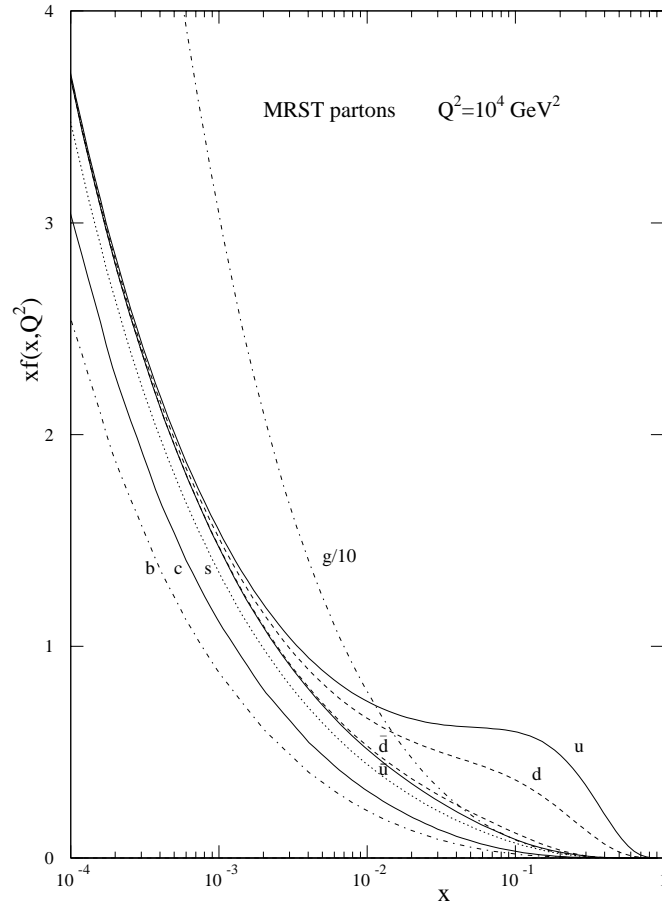

Fig. 9: The same parton distribution functions as in Fig. 8, but now at $\mu^2 = 10^4 \text{ GeV}^2$, from Ref. [27].

evolved to the much higher scale $\mu^2 = 10^4 \text{ GeV}^2$, typical of measurements at the HERA ep collider. By comparing the two figures one can clearly see the shrinkage to small x as Q^2 increases.

The precision of contemporary deep inelastic data demands that the QCD predictions are calculated beyond leading order. This amounts to the replacements (shown schematically):

$$P(x) \quad \rightarrow \quad P(x, Q^2) = P^{(0)}(x) + \frac{\alpha_S(Q^2)}{2\pi} P^{(1)}(x) + \dots$$

325

$$F = x \sum_q e_q^2 q \quad \rightarrow \quad F = x \sum_q (C_q * q + C_g * g)$$

$$C_q = e_q^2 \delta(1-x) + O(\alpha_S(Q^2)), \qquad C_g = O(\alpha_S(Q^2)). \tag{54}$$

The functions C_q and C_g are called coefficient functions. Beyond leading order, the definition of parton distributions (like the definition of α_S) becomes (factorization) scheme dependent (see Ref. [1] for a more detailed discussion). Different schemes have different coefficient and higher–order splitting functions, and correspondingly different parton distributions to render the (physical) structure functions scheme independent. In the 'DIS' scheme, for example, $C_q(x) = e_q^2 \delta(1-x)$, $C_g = 0$. It is conventional nowadays to work in the $\overline{\text{MS}}$ scheme, where for example

$$
\begin{aligned}
x^{-1} F_2^{\mu p}(x, Q^2) \;=\; & \sum_q e_q^2 \, q^{\overline{\text{MS}}}(x, Q^2) \\
& + \frac{\alpha_S^{\overline{\text{MS}}}(Q^2)}{2\pi} \sum_q \int_x^1 \frac{dz}{z} \, c_{2,q}(z) \, q^{\overline{\text{MS}}}\left(\frac{x}{z}, Q^2\right) \\
& + \left(\sum_q e_q^2\right) \frac{\alpha_S^{\overline{\text{MS}}}(Q^2)}{2\pi} \int_x^1 \frac{dz}{z} \, c_{2,g}(z) \, g^{\overline{\text{MS}}}\left(\frac{x}{z}, Q^2\right) \\
& + O(\alpha_S^2) \, .
\end{aligned}
\tag{55}
$$

The scaling violations predicted by perturbative QCD are clearly visible in the data. Figure 10 shows high precision data on the structure functions $F_2^{\nu N}$ and $x F_3^{\nu N}$ from the CCFR collaboration [29]. As expected, the slopes $\partial F_{2,3}/\partial \ln Q^2$ are negative at large x and positive at small x respectively. From data such as those shown in Fig. 10, the predictions of perturbative QCD for scaling violations (48) can be tested, and a precise measurement [29] of the strong coupling $\alpha_S(Q^2)$ can be made:

$$\text{CCFR}(F_{2,3}) \; : \quad \alpha_S(M_Z^2) = 0.119 \pm 0.002(\text{exp.}) \pm 0.001(\text{HT}) \pm 0.004(\text{scale}). \tag{56}$$

The second error is from an estimate of the higher–twist contribution:[6]

$$F(x, Q^2) \;=\; F^{(2)}(x, Q^2) \;+\; \frac{F^{(4)}(x, Q^2)}{Q^2} \;+\; \dots \, , \tag{57}$$

using the model of Ref. [30], and the third is the scale dependence uncertainty. Notice that, except at large x, the Q^2 variation of F_2 is sensitive to the *a priori* unknown gluon distribution and there is potentially a strong α_S–gluon correlation. Non–singlet structure functions such as F_3 do not suffer from the gluon correlation problem (see Eq. (48)), but these are only measurable experimentally by constructing differences between cross sections, e.g. $\sigma^{\nu N} - \sigma^{\bar{\nu}N}$. This inevitably introduces additional systematic and statistical uncertainties. The α_S value (56) is one of the most precise determinations, see Fig. 1. It agrees perfectly with the values measured in $e^+ e^-$ annihilation, showing that α_S is indeed a universal parameter, independent of whether the short distance process is spacelike (DIS) or timelike ($e^+ e^-$).

Deep inelastic fixed–target experiments measure quark distributions very accurately over a broad range in x ($\sim 0.01 - 0.8$) up to scales of order $\mu^2 \sim 200$ GeV^2. The HERA high-energy $e^\pm p$ collider, with $\sqrt{s} \sim 300$ GeV, is able to extend the x range down to very small values, and the Q^2 range up to very high values, see Fig. 11 [35]. At the high $Q^2 > \mathcal{O}(10^4 \text{ GeV}^2)$ values measured at HERA, the W and Z contributions to the ep cross sections cannot be neglected. The neutral current cross section (42) must be modified to include Z exchange, and a corresponding charged current cross section (for $ep \rightarrow \nu X$) introduced. Ignoring the proton mass, the expressions are:

---

[6]The superscripts on the right–hand side of (57) refer to the 'twist' = (dimension − spin) of the contributing operators.
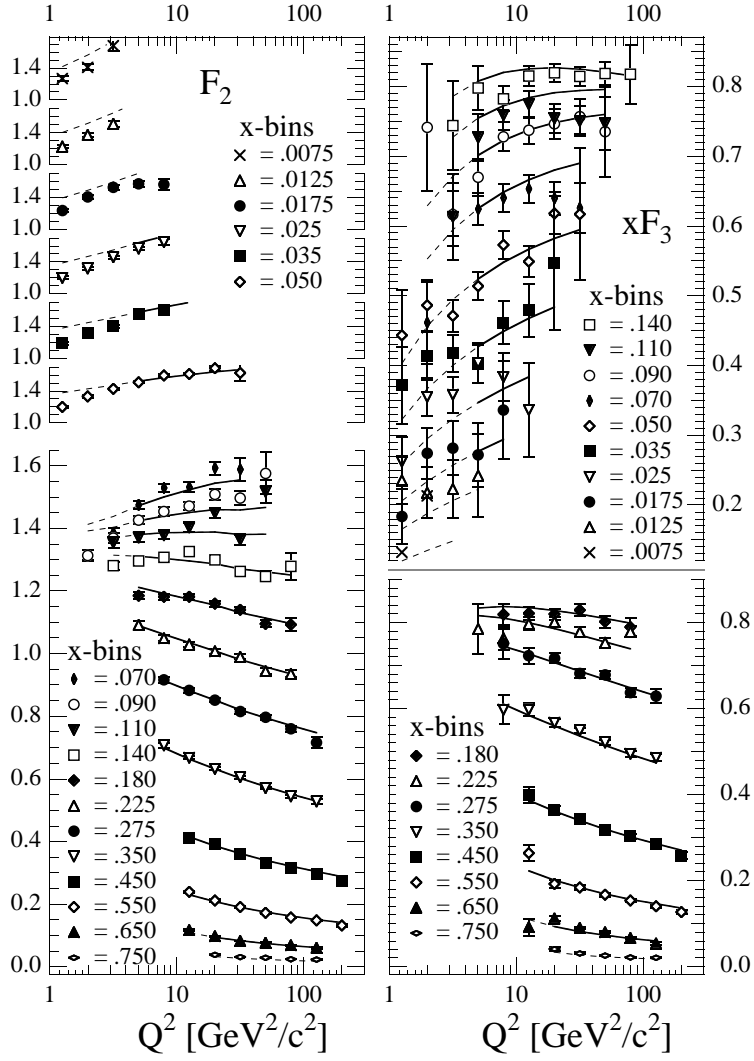
Fig. 10: Measurements of the structure function $F_2^{\nu N}$ from the CCFR collaboration together with a NLO QCD fit, from Ref. [29].

- <u>neutral current</u>

$$
\frac{d^2\sigma_{NC}(e^{\pm}p)}{dxdQ^2} = \frac{2\pi\alpha^2}{xQ^4}\left[[1+(1-y)^2]F_2(x,Q^2) - y^2F_L(x,Q^2)\right.
$$
$$
\left.\mp 2y(1-y)xF_3(x,Q^2)\right] \tag{58}
$$

$$
F_2(x,Q^2) = \sum_q[xq(x,Q^2) + x\bar{q}(x,Q^2)]\,A_q(Q^2)
$$
$$
xF_3(x,Q^2) = \sum_q[xq(x,Q^2) - x\bar{q}(x,Q^2)]\,B_q(Q^2) \tag{59}
$$

$$
A_q(Q^2) = e_q^2 - 2e_q v_e v_q P_Z + (v_e^2 + a_e^2)(v_q^2 + a_q^2)P_Z^2
$$
$$
B_q(Q^2) = -2e_q a_e a_q P_Z + 4v_e a_e v_q a_q P_Z^2
$$
$$
P_Z = \frac{Q^2}{Q^2 + M_Z^2}\frac{\sqrt{2}G_\mu M_Z^2}{4\pi\alpha} \tag{60}
$$

327
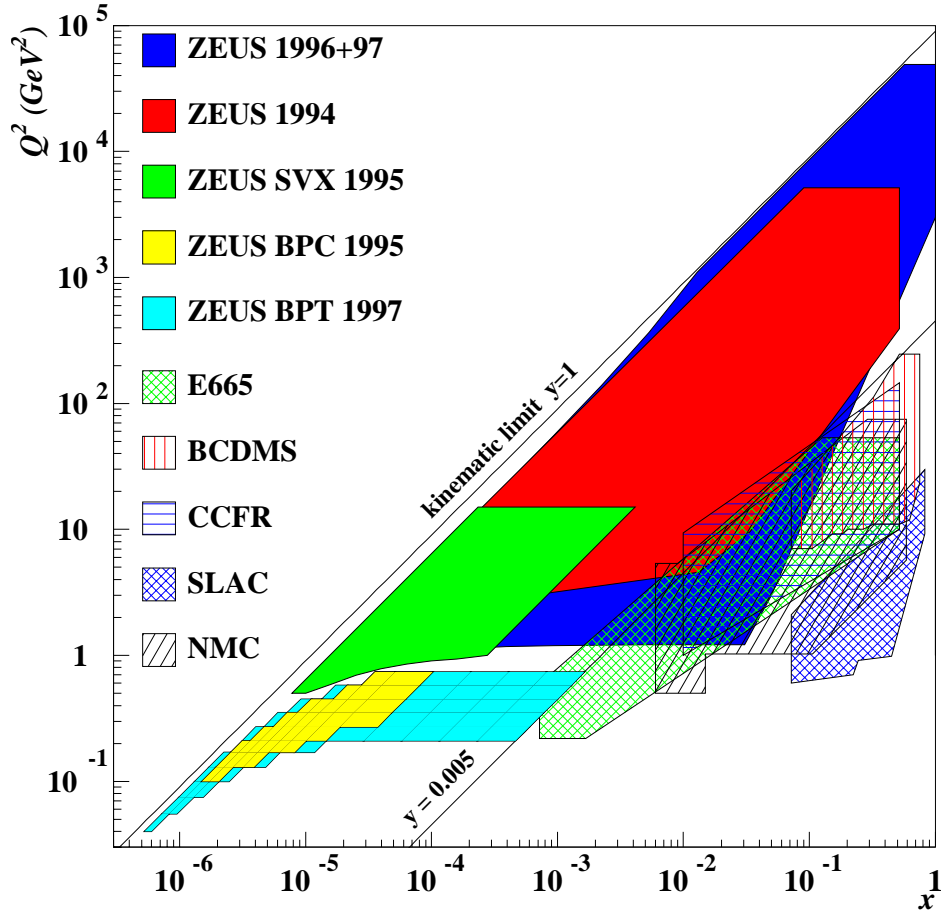
Fig. 11: Regions in the $x - Q^2$ plane covered by various deep inelastic scattering experiments.

- <u>charged current</u>

$$
\frac{d^2\sigma_{CC}(e^-p)}{dxdQ^2} = [1 - \mathcal{P}_e]\frac{G_\mu^2}{2\pi}\Big(\frac{M_W^2}{Q^2 + M_W^2}\Big)^2
$$
$$
\times \sum_{i,j} \Big[|V_{u_id_j}|^2 u_i(x, Q^2) + (1 - y)^2|V_{u_jd_i}|^2\bar{d}_i(x, Q^2)\Big]
$$
(61)

$$
\frac{d^2\sigma_{CC}(e^+p)}{dxdQ^2} = [1 + \mathcal{P}_e]\frac{G_\mu^2}{2\pi}\Big(\frac{M_W^2}{Q^2 + M_W^2}\Big)^2
$$
$$
\times \sum_{i,j} \Big[|V_{u_id_j}|^2 \bar{u}_i(x, Q^2) + (1 - y)^2|V_{u_jd_i}|^2 d_i(x, Q^2)\Big]
$$
(62)

From these expressions we see that (i) the charged current cross section is suppressed by $\mathcal{O}(Q^4)$ at small Q^2 where the neutral current cross section is dominated by photon exchange, and (ii) at very high $Q^2 \gg \mathcal{O}(M_V^2)$, the charged and neutral cross sections are of the same order. The HERA data confirm this behaviour: Fig. 12 shows the neutral and charged current cross sections for e^+p scattering at high Q^2 measured by ZEUS [36], together with the Standard Model predictions.

Parton distributions at some starting scale μ_0^2 are a byproduct of DGLAP fits to DIS data. These can then be evolved to higher μ^2 and used for hadron collider phenomenology. Instead of laboriously
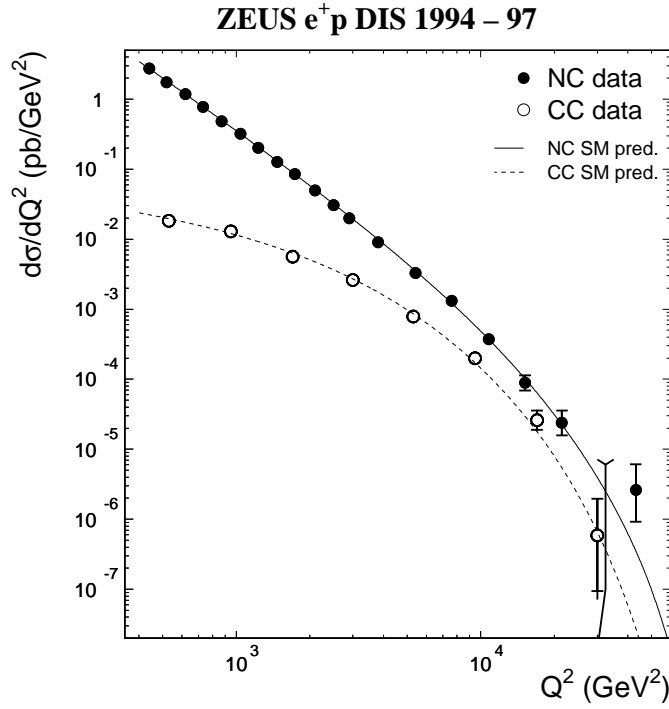
ZEUS e⁺p DIS 1994 – 97

Fig. 12: Charged and neutral current DIS cross sections at high Q^2, as measured by the ZEUS collaboration [36] in $e^+ p$ scattering at HERA.

integrating the DGLAP equations each time a parton distribution is required, it is useful to have an analytic approximation, valid to a sufficient accuracy over a prescribed (x, μ^2) range. Such parametrizations are discussed in the following section.

4.3 Parton distributions in hadrons

As we have seen in the previous sections, the distributions of quarks (and, indirectly via the DGLAP equations, gluons) in the proton are determined by values of the structure functions $F_i(x, Q^2)$ measured in the various deep inelastic scattering experiments. It is relevant to ask why we should devote so much effort to the study of the distributions of partons in the proton. There are two main reasons, one experimental and one theoretical. First, a detailed knowledge of parton distribution functions (pdfs) is an essential ingredient in all 'hard' interactions involving protons, and so they are needed to estimate the production rates of the various hard processes that may occur at present and future colliders. Second, the parton structure, as encoded in the f_i, is interesting in its own right. In particular, novel perturbative QCD effects are expected to become apparent at small x. The reason is that at small x the sum over soft gluons emitted off the incoming parton leads to a power series in $\alpha_S \ln(1/x)$, which on resummation, via the Lipatov (or BFKL) equation [31], suggests that the gluon and quark singlet distributions behave as

$$ xg, \ xq_S \ \sim \ x^{-\lambda} \tag{63} $$

as $x \to 0$, with $\lambda = 12 \ln 2 \alpha_S / \pi$ predicted to be about 0.5. Such an increase in $xg(x, \mu^2)$ and $xq_S(x, \mu^2)$ as x decreases cannot go on indefinitely. If the density of gluons becomes too large they can no longer be treated as free partons, and the effects of recombination or shadowing must be included. The 'naive' BFKL predictions (63) for the small x behaviour of the parton distributions is valid only for *asymptotically small x* values. It is far from clear whether the values attainable at HERA (see Fig. 11) are in fact small

Table 4: Processes studied in the global MRST analysis [27] (* indicates data fitted).

Process/ Experiment	Leading order subprocess	Parton behaviour probed
DIS ($\mu N \to \mu X$) $F_2^{\mu p}, F_2^{\mu d}, F_2^{\mu n}/F_2^{\mu p}$ (SLAC, BCDMS, NMC, E665)*	$\gamma^* q \to q$	Four structure functions $\to$ $u + \bar{u}$ $d + \bar{d}$ $\bar{u} + \bar{d}$
DIS ($\nu N \to \mu X$) $F_2^{\nu N}, x F_3^{\nu N}$ (CCFR)*	$W^* q \to q'$	s (assumed $= \bar{s}$), but only $\int x g(x, Q_0^2) dx \simeq 0.35$ and $\int (\bar{d} - \bar{u}) dx \simeq 0.1$
DIS (small x) F_2^{ep} (H1, ZEUS)*	$\gamma^*(Z^*) q \to q$	λ $(x\bar{q} \sim x^{-\lambda_S},\ xg \sim x^{-\lambda_g})$
DIS (F_L) NMC, HERA	$\gamma^* g \to q\bar{q}$	g
$\ell N \to c\bar{c} X$ F_2^c (EMC; H1, ZEUS)*	$\gamma^* c \to c$	c $(x \gtrsim 0.01;\ x \lesssim 0.01)$
$\nu N \to \mu^+ \mu^- X$ (CCFR)*	$W^* s \to c$ $\hookrightarrow \mu^+$	$s \approx \frac{1}{4}(\bar{u} + \bar{d})$
$pN \to \gamma X$ (WA70*, UA6, E706, …)	$qg \to \gamma q$	g at $x \simeq 2p_T^\gamma/\sqrt{s} \to$ $x \approx 0.2 - 0.6$
$pN \to \mu^+ \mu^- X$ (E605, E772)*	$q\bar{q} \to \gamma^*$	$\bar{q} = ...(1-x)^{\eta_S}$
$pp, pn \to \mu^+ \mu^- X$ (E866, NA51)*	$u\bar{u}, d\bar{d} \to \gamma^*$ $u\bar{d}, d\bar{u} \to \gamma^*$	$\bar{u} - \bar{d}\ (0.04 \lesssim x \lesssim 0.3)$
$ep, en \to e\pi X$ (HERMES)	$\gamma^* q \to q$ with $q = u, d, \bar{u}, \bar{d}$	$\bar{u} - \bar{d}\ (0.04 \lesssim x \lesssim 0.2)$
$p\bar{p} \to W X (Z X)$ (UA1, UA2; CDF, D0)	$ud \to W$	u, d at $x \simeq M_W/\sqrt{s} \to$ $x \approx 0.13;\ 0.05$
$\to \ell^\pm$ **asym** (CDF)*		slope of u/d at $x \approx 0.05 - 0.1$
$p\bar{p} \to t\bar{t} X$ (CDF, D0)	$q\bar{q}, gg \to t\bar{t}$	q, g at $x \gtrsim 2m_t/\sqrt{s} \simeq 0.2$
$p\bar{p} \to \text{jet} + X$ (CDF, D0)	$gg, qg, qq \to 2j$	q, g at $x \simeq 2E_T/\sqrt{s} \to$ $x \approx 0.05 - 0.5$

enough for the leading behaviour to be observable. Indeed, standard NLO DGLAP evolution provides a satisfactory explanation of the observed small–x behaviour, with approximately flat (i.e. $xf_i \sim x^0$) distributions at a starting scale $\mu_0^2 \sim 1$ GeV^2, see the discussion in Ref. [27] for example.

In fact, approximately flat starting distributions are in line with longstanding non–perturbative Regge arguments for structure functions in the $x \to 0$ limit. According to Regge theory, the high–energy behaviour of an elastic hadron scattering amplitude is controlled by a sequence of Regge trajectories corresponding to the exchange of families of particles with different spin, see for example Ref. [37]. In the small–x limit, the quark–proton amplitude $\mathcal{A}_{qp}$ in deep inelastic scattering is probed at high energy, $s \sim Q^2/x$, for which we would expect

$$\mathcal{A}_{qp} \sim \beta_\mathcal{P} s^{\alpha_\mathcal{P}-1} + \beta_\mathcal{R} s^{\alpha_\mathcal{R}-1} + \dots , \tag{64}$$

where the leading trajectories are

$$\begin{aligned} \alpha_\mathcal{P} &\simeq 1 & \text{pomeron } \mathcal{P} \\ \alpha_\mathcal{R} &\simeq \frac{1}{2} & \rho, \omega, a_2, f_2, \dots \end{aligned} \tag{65}$$

Inserting this behaviour into the parton–model calculation of the F_2 structure function gives the leading small–x behaviour

$$F_2(x) \sim \beta_\mathcal{P} x^{1-\alpha_\mathcal{P}} + \beta_\mathcal{R} x^{1-\alpha_\mathcal{R}} . \tag{66}$$

We may interpret the two terms in (66) as the contributions to the structure function from the flavour–singlet quark sea, with behaviour determined by the leading 'pomeron' trajectory $\alpha_\mathcal{P}$, and from the flavour–non–singlet valence quarks, with behaviour controlled by the 'Reggeon' trajectory $\alpha_\mathcal{R}$. We would likewise expect that the behaviour of the gluon distribution at small x is also determined by the pomeron trajectory, yielding the predictions

$$q_S, \ g \sim x^{-1}, \qquad q_V \sim x^{-\frac{1}{2}} \tag{67}$$

in the $x \to 0$ limit, or equivalently

$$F_2^p \sim x^0, \qquad F_2^p - F_2^n \sim x^{\frac{1}{2}} . \tag{68}$$

A detailed analysis of small x, modest Q^2 structure function measurements at HERA collider and fixed–target energies shows that they are indeed approximately consistent with the predictions of Regge theory, see for example the recent ZEUS measurements [35] of F_2 at small x in Fig. 13. However the data also show an apparent steepening of the behaviour at small x as Q^2 increases, exactly as expected from perturbative QCD DGLAP evolution as described above. Therefore, although much has been written about the theoretical 'BFKL' behaviour of the small–x parton distributions,[7] there is as yet no compelling experimental evidence and so we shall not discuss this further here.

There are currently three collaborations producing sets of parton distributions that are widely used in high-energy collider phenomenology: MRST (Martin–Roberts–Stirling-Thorne), CTEQ (Collaboration for Theoretical and Experimental Studies in Quantum Chromodynamics) and GRV (Glück–Reya–Vogt) (see, respectively, [27, 32, 33] and references therein). The first two of these use the concept of 'global fits' to determine each parton distribution as accurately as possible from high-precision data on deep inelastic structure functions and other hard scattering processes. The GRV analysis is in the context of the 'dynamical parton model' [34] in which the partons evolve from valence–like distributions at a low Q^2 scale. These starting distributions are tuned to fit the data at higher Q^2.

The last few years have seen a spectacular improvement in the precision and in the kinematic range of the experimental measurements of deep inelastic and related hard scattering processes. As a consequence the pdfs are much better known, with tight constraints on the gluon and the quark sea for Bjorken

---

[7]For a review of small–x physics, and a list of references, see for example Ref. [1].
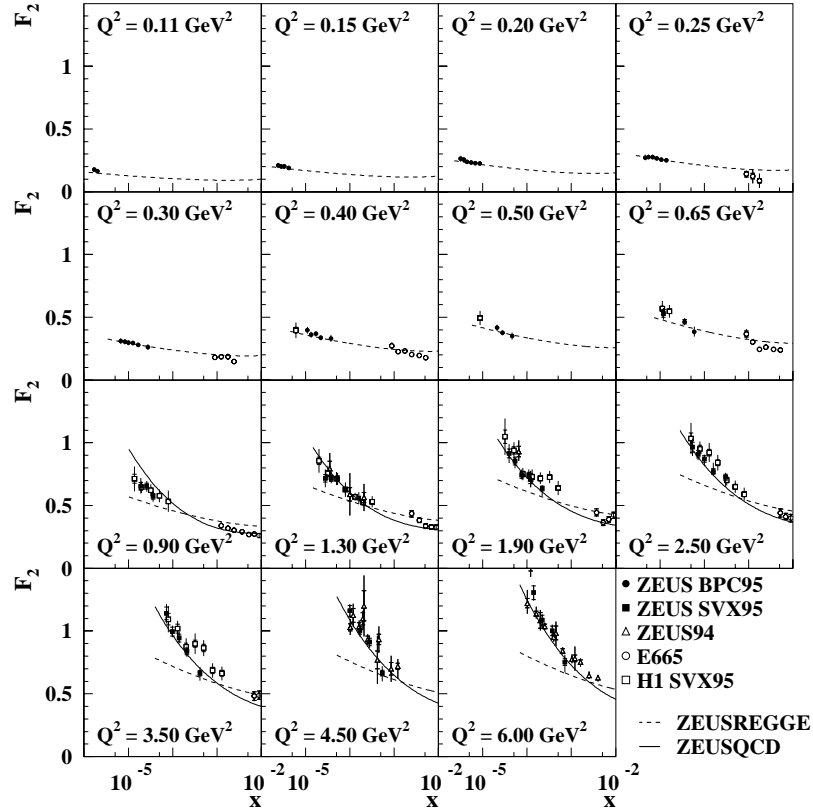
ZEUS 1995

Fig. 13: Low–Q^2 F_2 data for different Q^2 bins together with a Regge fit (dashed curves) to the ZEUS BPC95 data [35]. Also shown at larger values of Q^2 is the ZEUS NLO DGLAP fit (full curves).

x as low as 10^{-5}. In what follows we will summarize the recent MRST pdf analysis of Ref. [27]. This is the most recent of the global analyses, and takes into account all the new information as well as incorporating new theoretical developments in the heavy quark sector.

Table 4 illustrates the variety of data used in the recent MRST analysis [27]. The basic procedure is to parametrize the f_i at a sufficiently large 'starting scale' ($Q_0^2 = 1$ GeV^2 for MRST) so that the $f_i(x, Q^2)$ can be calculated reliably at higher Q^2 from perturbative QCD via the NLO DGLAP equations. Interestingly, the data are well described by remarkably simple parametrizations of parton distributions at the starting scale; in total only about 20 parameters are required. The generic form for each individual starting distribution can be taken to be

$$xf_i(x, Q_0^2) = A_i x^{-\lambda_i}(1 + \epsilon_i \sqrt{x} + \gamma_i x)(1 - x)^{\eta_i}, \tag{69}$$

with some of the A_i constrained by the sum rules in Eq. (45) and the remainder constrained by the fitting procedure.

The deep–inelastic structure functions directly pin down the valence and sea quark distributions, but information on the gluon distribution is more elusive. The momentum sum rule indicates that the gluon carries just less than 50% of the proton's momentum at Q_0^2. In addition, at small x the Q^2 evolution of the structure function is completely dominated by the gluon term:

$$\frac{\partial F_2(x, Q^2)}{\partial \ln Q^2} \approx \frac{\alpha_S(Q^2)}{2\pi} 2 \sum_q e_q^2 \int_x^1 \frac{dy}{y} \left(\frac{x}{y}\right) P_{qg}\left(\frac{x}{y}\right) yg(y, Q^2). \tag{70}$$

332

Therefore, while F_2 measures the quarks, its Q^2 derivative measures the gluon.

To obtain information on the gluon distribution at large x, input from other processes is needed. For example, in prompt photon production in hadron-hadron (pN) collisions the gluon enters at leading order via the QCD subprocess $gq \rightarrow \gamma q$, in contrast to $p\bar{p} \rightarrow \gamma X$ where the annihilation process $q\bar{q} \rightarrow \gamma g$ is much more important. The relevant data are from the WA70 and E706 collaborations [38, 39], which determine the gluon in the region $x \sim 0.2 - 0.5$. Combined with the momentum sum rule constraint, this gives a reasonable measurement of the gluon at large x, see Fig. 14, although additional assumptions are needed concerning the 'intrinsic transverse momentum' distribution of the partons in the proton, see for example the discussion in [27]. Data on the Drell–Yan $pN \rightarrow \mu^+\mu^- X$ process, which is mediated at LO by $q_{\mathrm{val}}\bar{q}_{\mathrm{sea}} \rightarrow \gamma^*$, constrain the large–$x$ $(1-x)^{\eta_s}$ behaviour of the sea quark distributions, see Section 5. Finally data on the rapidity distribution of charged leptons from W production and decay at the Tevatron $\bar{p}p$ collider impose tight constraints on the u and d distributions, particularly when the accurate measurements of $F_2^{\mu n}/F_2^{\mu p}$ have to be fitted simultaneously [27].
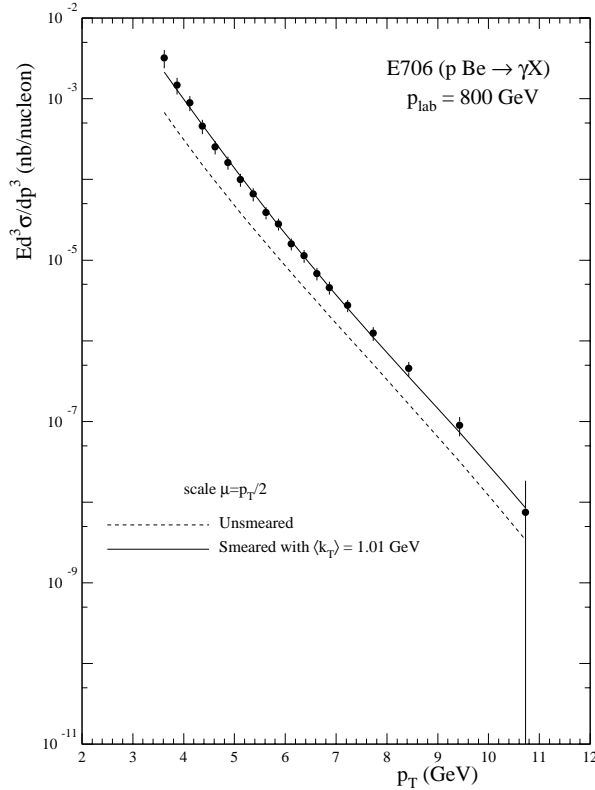

Fig. 14: Comparison of the E706 prompt photon data [39] data at 800 GeV with the MRST parton set [27]. The scale is chosen to be $p_T/2$ and the effect of including parton transverse momentum is shown. These data are used to constrain the large–x gluon.

As mentioned already, a feature of recent parton determinations is the marked difference between the $\bar{u}$ and $\bar{d}$ pdfs, see Fig. 8, motivated by new precise experimental measurements. The DIS structure function measurements (of $F_2^{\mu p}$, $F_2^{\mu n}$, $F_2^{\nu N}$ and $xF_3^{\nu N}$) determine $(\bar{u} + \bar{d})$, but not $(\bar{u} - \bar{d})$. Historically the first indication of the $\bar{u} \neq \bar{d}$ flavour asymmetry of the sea came from the evaluation of the Gottfried sum

$$I_{\mathrm{GS}} \equiv \int_0^1 \frac{dx}{x} \left(F_2^{\mu p} - F_2^{\mu n} \right) \tag{71}$$

by NMC [40]. This gives information on the integral of $\bar{u} - \bar{d}$ and indicates that, on average, $\bar{d}$ is greater than $\bar{u}$.

For a direct determination of $\bar{u} - \bar{d}$ consider, for example, the asymmetry of Drell–Yan production in pp and pn collisions [41]

$$A_{\mathrm{DY}} \equiv \frac{\sigma_{pp} - \sigma_{pn}}{\sigma_{pp} + \sigma_{pn}} = \frac{1 - r}{1 + r}, \tag{72}$$

where $r = \sigma_{pn}/\sigma_{pp}$ and where $\sigma \equiv d^2\sigma/dM\,dx_F$ with M and x_F being the invariant mass and the Feynman x of the produced lepton pair. At leading order we have

$$r \equiv \frac{\sigma_{pn}}{\sigma_{pp}} = \frac{(4u_1\bar{d}_2 + d_1\bar{u}_2 + 4\bar{u}_1 d_2 + \bar{d}_1 u_2 + 2s_1 s_2 + 8c_1 c_2)}{(4u_1\bar{u}_2 + d_1\bar{d}_2 + 4\bar{u}_1 u_2 + \bar{d}_1 d_2 + 2s_1 s_2 + 8c_1 c_2)} \tag{73}$$

where the pdfs are evaluated at $x_1, x_2 = (\pm x_F + \sqrt{x_F^2 + 4\tau})/2$, with $\tau = M^2/s$. We may rearrange the expression for $1 - r$, and hence that for A_{DY}, to show that it is dependent on the combinations $(\bar{u}_1 - \bar{d}_1)$ and $(\bar{u}_2 - \bar{d}_2)$.

The first experiment of this type was performed by the NA51 collaboration [42] who measured

$$R_{dp} \equiv \frac{\sigma_{pd}}{2\sigma_{pp}} = \frac{1}{2}(1 + r) \tag{74}$$

at $x_1 = x_2 = 0.18$ and found $A_{\mathrm{DY}} = -0.09 \pm 0.02 \pm 0.025$, which corresponds to $\bar{d}/\bar{u} \simeq 2$. Subsequently the E866 collaboration [43] measured R_{dp} over a much wider range of M and x_F, which enables a study of the x dependence of $(\bar{u} - \bar{d})$ over the range $0.04 < x < 0.3$. The continuous curve in Fig. 15 shows the MRST fit to these data. The dotted curve shows the values that would be obtained for the ratio if we were to set $\bar{u}$ equal to $\bar{d}$. The implications for $\bar{d}$ and $\bar{u}$ from the MRST fit to the E866 data are shown in Fig. 8.
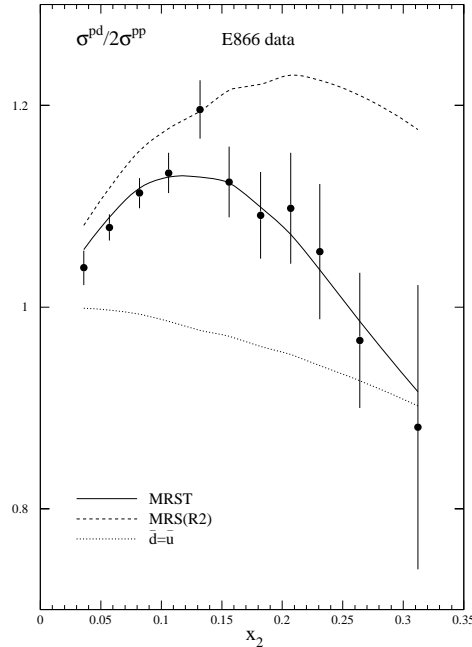

Fig. 15: The continuous curve is the MRST description of the E866 [43] data for the ratio of the cross sections for hadroproduction of dileptons for proton and deuterium targets versus x_2, the fractional momentum of the parton in the target. The other curves are for comparison only.

5. HARD PROCESSES IN HADRONIC COLLISIONS

5.1 Introduction

It was first pointed out by Drell and Yan [44] that parton model ideas developed for deep inelastic scattering could be extended to certain processes in hadron-hadron collisions. The paradigm process was the production of a massive lepton pair by quark-antiquark annihilation — the Drell–Yan process — and the hadronic cross section σ was to be obtained by weighting the subprocess cross section $\hat{\sigma}$ for $q\bar{q} \to \mu^+\mu^-$ with the parton distribution functions $f_{q/A}(x)$ extracted from deep inelastic scattering:

$$\sigma_{AB} = \int dx_a dx_b \, f_{a/A}(x_a) f_{b/B}(x_b) \, \hat{\sigma}_{ab \to X} \,, \tag{75}$$

where for the Drell–Yan process, $X = l^+l^-$ and $ab = q\bar{q}, \, \bar{q}q$. The domain of validity is the asymptotic 'scaling' limit (the analogue of the Bjorken scaling limit in deep inelastic scattering) $M_X \equiv M^2_{l^+l^-}, s \to \infty, \tau = M^2_{l^+l^-}/s$ fixed. The good agreement between theoretical predictions and the measured cross sections provided confirmation of the parton model formalism, and allowed for the first time a rigorous, quantitative treatment of hadronic cross sections. Studies were extended to other 'hard scattering' processes, for example the production of hadrons and photons with large transverse momentum, with equally successful results. Problems, however, appeared to arise when perturbative corrections from real and virtual gluon emission were calculated. Large logarithms from gluons emitted collinear with the incoming quarks appeared to spoil the convergence of the perturbative expansion. It was subsequently realised that these logarithms were the same as those that arise in deep inelastic scattering structure function calculations (see Section 4.), and could therefore be absorbed, via the DGLAP equations, in the definition of the parton distributions, giving rise to logarithmic violations of scaling. The key point was that *all* logarithms appearing in the Drell–Yan corrections could be factored into renormalized parton distributions in this way, and *factorization theorems* which showed that this was a general feature of hard scattering processes were derived [45]. Taking into account the leading logarithm corrections, Eq. (75) simply becomes:

$$\sigma_{AB} = \int dx_a dx_b \, f_{a/A}(x_a, Q^2) f_{b/B}(x_b, Q^2) \, \hat{\sigma}_{ab \to X} \,. \tag{76}$$

The Q^2 that appears in the pdfs is a large momentum scale that characterizes the hard scattering, e.g. $M^2_{l^+l^-}, p^2_T, \dots$. Changes to the Q^2 scale of $\mathcal{O}(1)$ are equivalent in this leading logarithm approximation.

The final step in the story was the recognition that the *finite* corrections left behind after the logarithms had been factored were not universal and had to be calculated separately for each process, giving rise to $\mathcal{O}(\alpha_S)$ corrections to the leading logarithm cross section of (76). Schematically

$$\sigma_{AB} = \int dx_a dx_b \, f_{a/A}(x_a, M^2) \, f_{b/B}(x_b, M^2) \, \times \, [\, \hat{\sigma}_0 \, + \, \alpha_S(\mu^2) \, \hat{\sigma}_1 \, + \, \dots \,]_{ab \to X} \,. \tag{77}$$

Here M^2 is the *factorization scale* and μ^2 is the renormalization scale for the QCD running coupling. Formally, the perturbation series is invariant under changes in these parameters, the M and μ dependence of the coefficients, e.g. $\hat{\sigma}_1$, exactly compensating the explicit dependence of the parton distributions and the coupling constant. This compensation becomes more exact as more terms are included in the perturbation series. To avoid unnaturally large logarithms reappearing in the perturbation series it is sensible to choose M and μ values of the order of the typical momentum scales of the hard scattering process, and $M = \mu$ is also often assumed.

In general, all the important hadronic processes have now been calculated to next–to–leading order (NLO), i.e. up to and including the $\hat{\sigma}_1$ terms. One process — the Drell–Yan process — is even calculated to one order higher (see below). This allows a very high degree of precision in a wide variety of processes. In many cases, the residual renormalization and factorization scale dependence is weak, and the precision of the theoretical prediction is limited only by uncertainties in the knowledge of the parton distributions.

335

What, then, are the most important applications of this formalism? One can, for example, attempt to measure α_S, particularly from those processes involving α_S at leading order, i.e. in $\hat{\sigma}_0$, and also study final–state QCD jets in parton scattering processes. One can also obtain information on parton distributions, particularly the gluon and sea quark distributions, complementary to that from deep inelastic scattering, as described in the previous section. However, perhaps the most important application is the prediction of various Standard Model and New Physics cross sections at high energy colliders such as the Tevatron ($p\bar{p}$) and LHC (pp). There are many examples of situations where the ability to detect a signal for new particle production depends crucially on the accuracy of the Standard Model background estimate. For reference, we show in Fig. 16 the predictions for some important Standard Model cross sections at $p\bar{p}$ and pp colliders, calculated at next–to–leading order in QCD perturbation theory using the latest MRST pdfs [27].[8]

We have already mentioned that the Drell–Yan process is the paradigm hadron–collider hard scattering process, and so we will discuss this in some detail in what follows. Many of the remarks apply also to other processes, in particular those shown in Fig. 16, although of course the higher–order corrections and the initial–state parton combinations are process dependent.

5.2 The Drell–Yan process

The Drell–Yan process is the production of a lepton pair (e^+e^- or $\mu^+\mu^-$ in practice) of large invariant mass M in hadron-hadron collisions by the mechanism of quark–antiquark annihilation [44]. In the basic Drell–Yan mechanism, a quark and antiquark annihilate to produce a virtual photon, $q\bar{q} \to \gamma^* \to l^+l^-$. At high energy colliders, such as the Tevatron and LHC, there is of course sufficient centre–of–mass energy for the production of on–shell W and Z bosons as well, see below. The cross section for quark-antiquark annihilation to a lepton pair via an intermediate massive photon is easily obtained from the fundamental QED $e^+e^- \to \mu^+\mu^-$ cross section, with the addition of the appropriate colour and charge factors.

$$\sigma(q\bar{q} \to e^+e^-) = \frac{4\pi\alpha^2}{3\hat{s}}\frac{1}{N}Q_q^2, \tag{78}$$

where Q_q is the quark charge: $Q_u = +2/3$, $Q_d = -1/3$ *etc*. The overall colour factor of $1/N = 1/3$ is due to the fact that only when the colour of the quark matches with the colour of the antiquark can annihilation into a colour–singlet final state take place.

In general, the incoming quark and antiquark will have a spectrum of centre–of–mass energies $\sqrt{\hat{s}}$, and so it is more appropriate to consider the differential mass distribution:

$$\frac{d\hat{\sigma}}{dM^2} = \frac{\hat{\sigma}_0}{N}Q_q^2\delta(\hat{s} - M^2), \quad \hat{\sigma}_0 = \frac{4\pi\alpha^2}{3M^2}, \tag{79}$$

where M is the mass of the lepton pair. In the centre–of–mass frame of the two hadrons, the components of momenta of the incoming partons may be written as

$$p_1^\mu = \frac{\sqrt{s}}{2}(x_1, 0, 0, x_1)$$
$$p_2^\mu = \frac{\sqrt{s}}{2}(x_2, 0, 0, -x_2) . \tag{80}$$

The square of the parton centre–of–mass energy $\hat{s}$ is related to the corresponding hadronic quantity by $\hat{s} = x_1 x_2 s$. Folding in the momentum distribution functions for the initial state quarks and antiquarks in the beam and target gives the hadronic cross section:

$$\frac{d\sigma}{dM^2} = \frac{\hat{\sigma}_0}{N} \int_0^1 dx_1 dx_2 \delta(x_1 x_2 s - M^2)$$
$$\times \left[\sum_k Q_k^2 (q_k(x_1, M^2)\bar{q}_k(x_2, M^2) + [1 \leftrightarrow 2]) \right] . \tag{81}$$

---

[8]Also shown, for comparison, is the *total* cross section calculated using a (non–perturbative) Regge–based model [2].

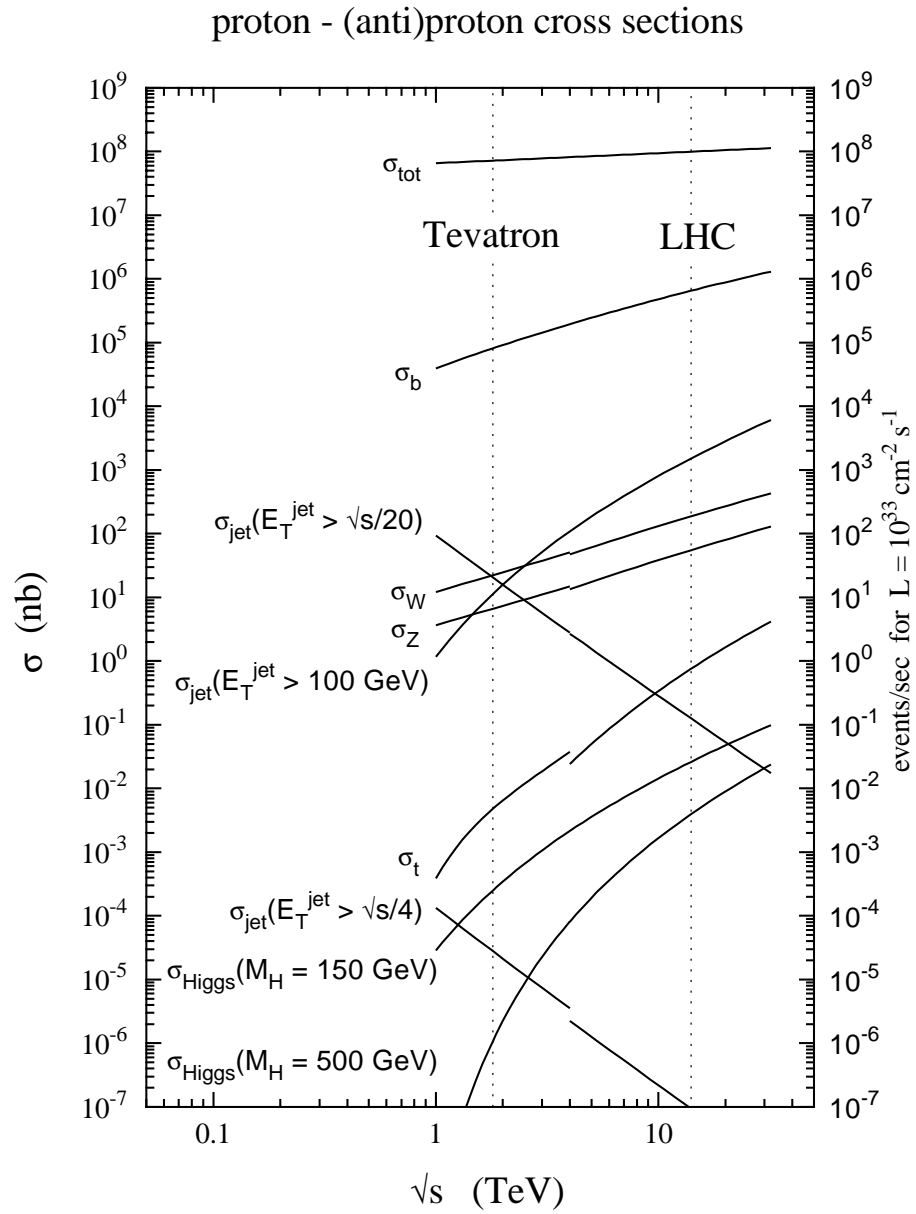# proton - (anti)proton cross sections

Fig. 16: Standard Model cross sections at the Tevatron and LHC colliders, calculated using MRST partons.

Note that the virtual photon is a *timelike* ($Q^2 > 0$) probe of the hadronic structure.

Apart from the mild logarithmic M^2 dependence in the distribution functions, the lepton–pair cross section exhibits *scaling* in the variable $\tau = M^2/s$:

$$
\begin{aligned}
M^3 \frac{d\sigma}{dM} &= \frac{8\pi\alpha^2\tau}{3N} \int_0^1 dx_1 dx_2 \delta(x_1 x_2 - \tau) \\
&\quad \times \left[\sum_k Q_k^2 (q_k(x_1, M^2) \bar{q}_k(x_2, M^2) + [1 \leftrightarrow 2]) \right] \\
&= F(\tau, M^2) .
\end{aligned}
\tag{82}
$$

From (80), the rapidity of the produced lepton pair is found to be $y = 1/2 \ln(x_1/x_2)$, and hence

$$
x_1 = \sqrt{\tau}\, e^y , \qquad x_2 = \sqrt{\tau}\, e^{-y}.
\tag{83}
$$

The double–differential cross section is therefore

$$
\frac{d\sigma}{dM^2 dy} = \frac{\hat{\sigma}_0}{Ns} \left[\sum_k Q_k^2 (q_k(x_1, M^2) \bar{q}_k(x_2, M^2) + [1 \leftrightarrow 2]) \right].
\tag{84}
$$

with x_1 and x_2 given by (83). By measuring the distribution in the rapidity and mass of the lepton pair one can in principle directly measure the quark distribution functions of the colliding hadrons, see below. This is particularly important for pion distributions, which are not accessible from deep inelastic scattering.

Another variable that is sometimes used is the longitudinal momentum fraction of the lepton pair $x = 2p_L/\sqrt{s}$. In the parton model, it follows from (80) that

$$
x = x_1 - x_2 ,
\tag{85}
$$

which leads to (*cf.* (83))

$$
x_1 = \frac{1}{2}\left(x + \sqrt{x^2 - 4\tau} \right) , \qquad x_2 = \frac{1}{2}\left(x - \sqrt{x^2 - 4\tau} \right) .
\tag{86}
$$

Both the cross sections $d\sigma/dM^2 dy$ and $d\sigma/dM^2 dx$ can therefore be used to probe the parton distributions. Note also that the ranges of the variables y and x are obtained by requiring $x_1, x_2 \leq 1$:

$$
-\frac{1}{2}\log\frac{1}{\tau} \leq y \leq \frac{1}{2}\log\frac{1}{\tau} , \qquad -1 + \tau \leq x \leq 1 - \tau .
\tag{87}
$$

As mentioned in the introduction to this section, in QCD there exists a systematic procedure for calculating the perturbative corrections to all orders. The next–to–leading order corrections are obtained from one–gluon real and virtual emission diagrams:

$$
\begin{aligned}
\frac{d\sigma}{dM^2} &= \frac{\sigma_0}{Ns} \int_0^1 dx_1 dx_2 dz \, \delta(x_1 x_2 z - \tau) \\
&\quad \left\{ \left[\sum_k Q_k^2 (q_k(x_1, \mu^2) \bar{q}_k(x_2, \mu^2) + [1 \leftrightarrow 2]) \right] \right. \\
&\quad \times \left[\delta(1-z) + \frac{\alpha_S(\mu^2)}{2\pi} f_q(z) \right] \\
&\quad + \left[\sum_k Q_k^2 (g(x_1, \mu^2)(q_k(x_2, \mu^2) + \bar{q}_k(x_2, \mu^2)) \right. \\
&\quad \left. \left. + [1 \leftrightarrow 2]) \right] \left[\frac{\alpha_S(\mu^2)}{2\pi} f_g(z) \right] \right\} ,
\end{aligned}
\tag{88}
$$

338

where μ is the (arbitrary) factorization/renormalization scale. Explicit expressions for the f_q and f_g correction terms [46] can be found, for example, in Ref. [1]. The $O(\alpha_S^2)$ corrections to $d\sigma/dM^2$ have also been calculated [47], but the expressions are again too cumbersome to be presented here.

The size of the perturbative corrections depends on the lepton–pair mass and on the overall centre–of–mass energy. At fixed–target energies and masses the correction is generally large and positive, of order 50% or more. In this regime of relatively large τ, the (negative) contribution from the quark-gluon scattering terms in (88) is quite small. However at $p\bar{p}$ and pp collider energies, where τ is much smaller, the f_g term is more important and the overall correction is smaller.

Several important pieces of information can be obtained from Drell–Yan data. Low–mass lepton–pair production in high energy hadron collisions is, at least in principle, sensitive to the small x behaviour of the parton distributions. In pp or pN collisions the cross section is proportional to the sea–quark distribution, $\bar{q}(x, Q^2)$. This provides complementary information to deep inelastic scattering, and in fact Drell–Yan data can be used to constrain the sea-quark distributions in global parton distribution fits.
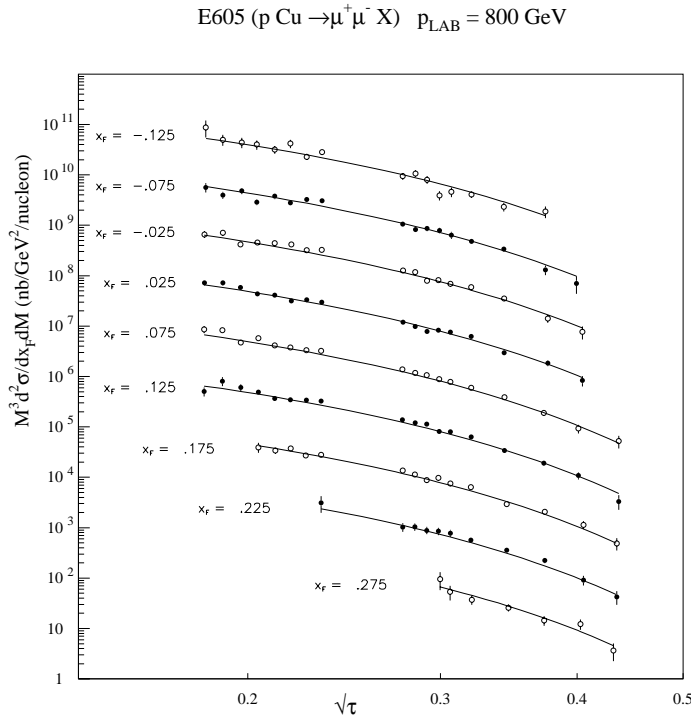

Fig. 17: Hadroproduction of dileptons computed from the MRST parton set compared with the E605 data [48]. The theory curves include an additional K' factor of 0.9. No correction for the heavy target has been made. The scale on the left–hand axis is appropriate for the theory and data at $x_F = -0.125$. For display purposes the normalization is then decreased by a factor of ten for each step upwards in x_F.

As an example, Fig. 17, from Ref. [27], shows a comparison of data from the E605 collaboration [48] on the cross section $M^3 d^2\sigma/dM dx_F$ for $p\,\mathrm{Cu} \to \mu^+\mu^-$ at $p_{\mathrm{lab}} = 800 \mathrm{\ GeV}/c\,(\sqrt{s} = 38.8 \mathrm{\ GeV})$ with theoretical (NLO QCD) predictions calculated at next–to–leading order. The data are used in the global MRST fit to constrain the sea quarks in the interval $0.15 \lesssim x \lesssim 0.4$. The factorization and renormalization scales are here set equal to the invariant mass M of the lepton pair, and an overall phenomenological normalization parameter, which allows for possible higher–order effects, is included.

Other important information can be obtained from Drell–Yan cross section measurements. The distributions of quarks in *pions* can be extracted from data in πp and πN collisions. The 'EMC effect (see Ref. [26]) — the apparent difference between quark distributions in light and heavy nuclei — can also

be studied in Drell–Yan processes. The transverse momentum of the lepton pair also gives direct information on the transverse momentum distribution of quarks with respect to the parent hadron direction. A comprehensive review of Drell–Yan phenomenology that describes these issues in more detail can be found in Ref. [49], for example.

If the hadron collider energy is large enough, the annihilation of the quarks and antiquarks can produce real W and Z bosons. Indeed the discovery in 1983 of the W and Z gauge bosons in this way at the CERN $p\bar{p}$ collider [50] provided dramatic confirmation of the Glashow–Salam–Weinberg electroweak model. The decay widths of the W and Z are only a few per cent of the boson masses, and so instead of the differential distribution in the resulting lepton pair ($l\nu$ or l^+l^-) invariant mass, it is more appropriate to consider the production cross section for the production of approximately stable on–shell particles with masses M_W and M_Z. These can then be multiplied by branching ratios for the various hadronic and leptonic final states. In analogy with the Drell–Yan cross section derived above, the subprocess cross sections for W and Z production are readily calculated to be

$$
\begin{aligned}
\hat{\sigma}^{q\bar{q}'\to W} &= \frac{\pi}{3}\sqrt{2}G_F M_W^2 |V_{qq'}|^2 \delta(\hat{s} - M_W^2) \\
\hat{\sigma}^{q\bar{q}\to Z} &= \frac{\pi}{3}\sqrt{2}G_F M_Z^2 (v_q^2 + a_q^2) \delta(\hat{s} - M_Z^2),
\end{aligned}
\tag{89}
$$

where $V_{qq'}$ is the appropriate Cabibbo–Kobayashi–Maskawa matrix element, and v_q (a_q) is the vector (axial vector) coupling of the Z to the quarks. The $O(\alpha_S)$ perturbative QCD correction to the W and Z cross sections is the same as the Drell–Yan correction (for a photon of the same mass) discussed in the previous section — the gluon is 'flavour blind' and couples in the same way to the annihilating quark and antiquark.
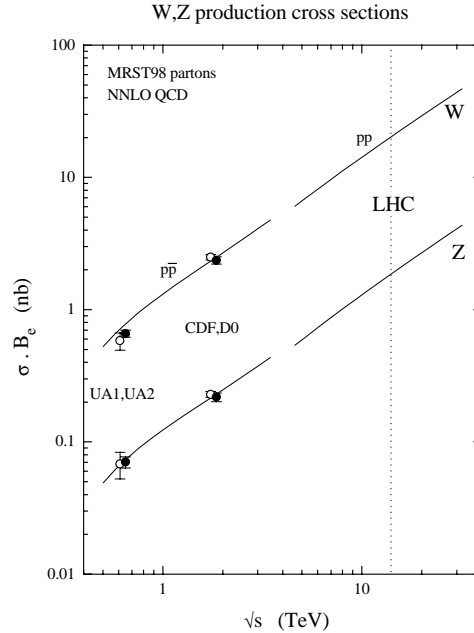

Fig. 18: Theoretical (NNLO QCD) predictions for the $W^{\pm}$ and Z^0 total production cross sections in pp and $p\bar{p}$ collisions, as a function of $\sqrt{s}$, with data from UA1 [51], UA2 [52], CDF [53] and D0 [54].

As already noted, these cross sections have now been calculated to next–to–next–to–leading order (i.e. $O(\alpha_S^2)$) [47]. Figure 18 shows the cross sections for $W^{\pm}$ and Z^0 production as a function of the collider energy $\sqrt{s}$. The curves are calculated using the results of Ref. [47] (in the $\overline{\text{MS}}$ scheme) with
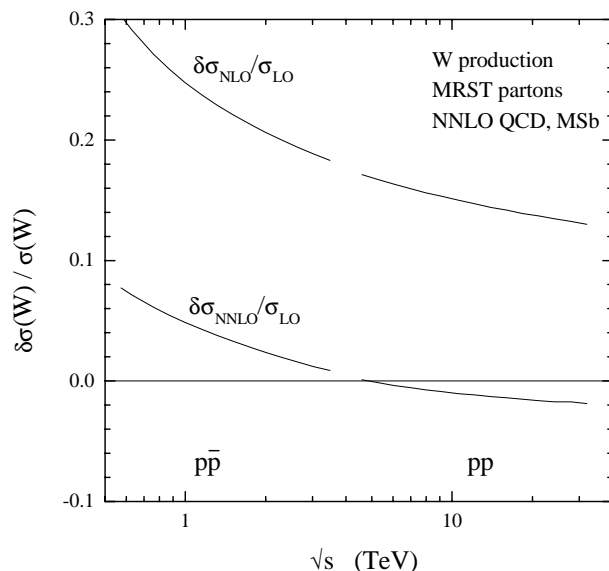
Fig. 19: The dependence of the NLO and NNLO corrections to the total W production cross section on the collider energy $\sqrt{s}$, in pp and $p\bar{p}$ collisions..

MRST parton distributions [27] and the renormalization and factorization scales $M = \mu = M_W, M_Z$. The data points are from UA1 [51], UA2 [52], CDF [53] and D0 [54] at $\sqrt{s} = 630$ GeV and 1.8 TeV. The net effect of the NLO and NNLO corrections is to increase the lowest order cross section by about 30%. The NLLO correction is significantly smaller than the NLO correction, due to a partial cancellation between the positive second order corrections involving the $q\bar{q}$ initial state and the negative corrections from the qg initial state, see Fig. 19. Perhaps the most important point to note from Fig. 18 is that, aside from unknown (and presumably small) $O(\alpha_S^3)$ corrections, there is virtually no theoretical uncertainty associated with the predictions — the parton distributions are being probed in a range of $x \sim M_W/\sqrt{s}$ where they are constrained from deep inelastic scattering, see Fig. 11, and the scale dependence is weak [27]. This overall agreement with experiment, therefore, provides a powerful test of the whole theoretical edifice that goes into the calculation.

Lack of space prevents a discussion of many other aspects of W and Z phenomenology at hadron colliders. The measurement of the W mass and width, the angular distributions of the lepton decay products etc. test the electroweak sector of the Standard Model and are complementary to the precision Z measurements made at LEP and SLC. The production of Drell–Yan (γ^*, W, Z) lepton pairs at large transverse momentum — mediated by the next–to–leading–order subprocesses $q\bar{q} \rightarrow Vg$ and $qg \rightarrow Vq$ — also provides an important test of perturbative QCD. A detailed discussion can be found in Ref. [1].

341

References

[1] *QCD and Collider Physics*, R.K. Ellis, W.J. Stirling and B.R. Webber, Cambridge University Press (1996).

[2] *Review of Particle Properties*, C. Caso *et al.*, Eur. Phys. J. **C2** (1998) 1, and 1999 off-year partial update for the 2000 edition available on the PDG WWW pages (URL: http://pdg.lbl.gov/).

[3] W.J. Marciano, Phys. Rev. **D29** (1984) 580.

[4] F. Bloch and A. Nordsieck, Phys. Rev. **52** (1937) 54.

[5] T. Kinoshita, J. Math. Phys. **3** (1962) 650.
T.D. Lee and M. Nauenberg, Phys. Rev. **B133** (1964) 1549.

[6] M.A. Samuel and L.R. Surguladze, Phys. Rev. Lett. **66** (1991) 560; **66** (1991) 2416(e).
S.G. Gorishny, A.L. Kataev and S.A. Larin, Phys. Lett. **B259** (1991) 144.

[7] B.A. Kniehl and J.H. Kuhn, Nucl. Phys. **B329** (1990) 547.

[8] LEP Electroweak Working Group report CERN-EP-2000-016 (2000).

[9] G. Grunberg, Phys. Lett. **B95** (1980) 70.

[10] P.M. Stevenson, Nucl. Phys. **B150** (1979) 357.

[11] JADE collaboration: S. Bethke *et al.*, Phys. Lett. **B213** (1988) 235.

[12] G. Kramer and B. Lampe, Fortschr. Phys. **37** (1989) 161.

[13] OPAL collaboration: G. Alexander *et al.*, Z. Phys. **C72** (1996) 191.

[14] OPAL collaboration: M.Z. Akrawy *et al.*, Phys. Lett. **B235** (1990) 389.

[15] S. Bethke, Z. Kunszt, D.E. Soper and W.J. Stirling, Nucl. Phys. **B370** (1992) 310.

[16] N. Brown and W.J. Stirling, Phys. Lett. **B252** (1990) 657.

[17] S. Catani, Yu.L. Dokshitzer, M. Olsson, G. Turnock and B.R. Webber, Phys. Lett. **269B** (1991) 432.

[18] DELPHI collaboration: P. Abreu *et al.*, Zeit. Phys. **C59** (1993) 21.

[19] L3 collaboration: M. Acciarri *et al.*, Phys. Lett. **B444** (1998) 569.

[20] B.R. Webber, Phys. Lett. **B339** (1994) 148.
Yu.L. Dokshitzer, G. Marchesini and B.R. Webber, Nucl. Phys. **B469** (1996) 93.
G.P. Korchemsky and G. Sterman, preprint hep-ph/9505391; Nucl. Phys. **B437** (1995) 415.
P. Nason and M.H. Seymour, Nucl. Phys. **B454** (1995) 291.
R. Akhoury and V.I. Zakharov, Phys. Lett. **B357** (1995) 646; Nucl. Phys. **B465** (1996) 295.
V.M. Braun, presented at 1996 Annual Divisional Meeting (DPF 96) of the Division of Particles and Fields of the American Physical Society, Minneapolis, August 1996, preprint hep-ph/9610212 (1996).
M. Beneke, presented at the 28th International Conference on High-Energy Physics (ICHEP 96), Warsaw, Poland, July 1996, preprint hep-ph/9609215 (1996).

[21] Yu.L. Dokshitzer and B.R. Webber, Phys. Lett. **B352** (1995) 451.

[22] Yu.L. Dokshitzer and B.R. Webber, Phys. Lett. **B404** (1997) 321.

[23] DELPHI collaboration: P. Abreu *et al.*, Phys. Lett. **B456** (1999) 322 .

[24] Yu.L. Dokshitzer, A. Lucenti, G. Marchesini and G.P. Salam, Nucl. Phys. **B511** (1997) 396; JHEP **9805** (1998) 003.

[25] H1 collaboration: C. Adloff *et al.*, preprint hep-ex/9912052 (1999).

[26] *The Structure of the Proton*, R.G. Roberts, Cambridge University Press (1990).

[27] A.D. Martin, R.G. Roberts, W.J. Stirling and R. Thorne, Eur. Phys. J. **C4** (1998) 463.

[28] L.N. Lipatov, Sov. J. Nucl. Phys. **20** (1975) 95.
V.N. Gribov and L.N. Lipatov, Sov. J. Nucl. Phys. **15** (1972) 438.
G. Altarelli and G. Parisi, Nucl. Phys. **B126** (1977) 298.
Yu.L. Dokshitzer, Sov. Phys. JETP **46** (1977) 641.

[29] CCFR collaboration: W.G. Seligman *et al.*, preprint hep-ex/9701017 (1997).

[30] M. Dasgupta and B.R. Webber, Eur. Phys. J. **C1** (1998) 539.

[31] E.A. Kuraev, L.N. Lipatov and V.S. Fadin, Phys. Lett. **B60** (1975) 50; Sov. Phys. JETP **44** (1976) 433 and **45** (1977) 199.
Ya.Ya. Balitsky and L.N. Lipatov, Sov. J. Nucl. Phys. **28** (1978) 822.

[32] CTEQ collaboration: H.-L. Lai *et al.*, Phys. Rev. **D55** (1997) 1280.

[33] M. Glück, E. Reya and A. Vogt, Zeit. Phys. **C67** (1995) 433.

[34] G. Altarelli, N. Cabibbo, L. Maiani and R. Petronzio, Nucl. Phys. **B69** (1974) 531.
M. Glück and E. Reya, Nucl. Phys. **B130** (1977) 76.

[35] ZEUS collaboration: J. Breitweg *et al.*, Eur. Phys. J. **C7** (1999) 609.

[36] ZEUS collaboration: J. Breitweg *et al.*, Eur. Phys. J. **C12** (2000) 411.

[37] P.D.B. Collins, *Introduction to Regge Theory*, Cambridge University Press (1977).

[38] WA70 collaboration: M. Bonesini *et al.*, Z. Phys. **C38** (1988) 371.

[39] E706 collaboration: L. Apanasevich *et al.*, Phys. Rev. Lett. **81** (1998) 2642.

[40] NMC collaboration: P. Amaudruz *et al.*, Phys. Rev. Lett. **66** (1991) 2712.

[41] S.D. Ellis and W.J. Stirling, Phys. Lett. **B256** (1991) 258.

[42] NA51 collaboration: A. Baldit *et al.*, Phys. Lett. **B332** (1994) 244.

[43] E866 collaboration: E.A. Hawker *et al.*, Phys. Rev. Lett. **80** (1998) 3715.

[44] S.D. Drell and T.M. Yan, Ann. Phys. **66** (1971) 578.

[45] See for example: J.C. Collins and D.E. Soper, Ann. Rev. Nucl. Part. Sci. **37** (1987) 383, and references therein.

[46] G. Altarelli, R.K. Ellis and G. Martinelli, Nucl. Phys. **B143** (1978) 521; **B146** (1978) 544(e); **B147** (1979) 461.
J. Kubar-Andre and F.E. Paige, Phys. Rev. **D19** (1979) 221.
J. Kubar-Andre, M. LeBellac, J.L. Meunier and G. Plaut, Nucl. Phys. **B175** (1980) 251.

[47] R. Hamberg, T. Matsuura and W.L. van Neerven, Nucl. Phys. **B345** (1990) 331; Nucl. Phys. **B359** (1991) 343.
W.L. van Neerven and E.B. Zijlstra, Nucl. Phys. **B382** (1992) 11.

[48] E605 collaboration: G. Moreno *et al.*, Phys. Rev. **D43** (1991) 2815.

[49] K. Freudenreich, Int. J. Mod. Phys **A19** (1990) 3643.

[50] UA1 collaboration: G. Arnison *et al.*, Phys. Lett. **B122** (1983) 103.
UA2 collaboration: G. Banner *et al.*, Phys. Lett. **B122** (1983) 476.

[51] UA1 collaboration: C. Albajar *et al.*, Z. Phys. **C44** (1989) 115.

[52] UA2 collaboration: J. Alitti *et al.*, Phys. Lett. **B276** (1992) 365.

[53] CDF collaboration: F. Abe *et al.*, Phys. Rev. Lett. **76** (1996) 3070.

[54] D0 collaboration: S. Abachi *et al.*, Phys. Rev. Lett. **75** (1995) 1456.